

1 First UK field application and performance of 2 microcapsule-based self-healing concrete

3
4 Abir Al-Tabbaa^a, Chrysoula Litina^{*a}, Petros Giannaros^{a1}, Antonios Kanellopoulos^{a2} and Livia
5 Souza^a
6

7 ^aDepartment of Engineering, University of Cambridge, Trumpington Road, Cambridge CB2 1PZ, UK
8

9 *Corresponding authors:

10 Chrysoula Litina, cl519@cam.ac.uk, Department of Engineering, University of Cambridge,
11 Trumpington Road, Cambridge CB2 1PZ, UK
12
13

14 Abstract

15 Maintaining the health and reliability of our infrastructure is of strategic importance. The current
16 state of the UK infrastructure, and the associated huge costs of inspection, maintenance, repair and
17 eventual replacement, is not sustainable and is no longer environmentally viable. The design of
18 infrastructure, mainly concrete, remains traditional and poor material performance continues to be
19 the main cause of deterioration and failure in our infrastructure systems. Biomimetic materials, that
20 emulate natural biological systems in their ability to self-healing, provide an exciting and plausible
21 solution. Embedding cementitious materials with in-built capabilities to sense and respond to their
22 environmental triggers could potentially eliminate all external interventions and deliver a resilience
23 infrastructure. The work presented in this paper forms part of a national initiative that has been
24 developing biomimetic cementitious infrastructure materials which culminated in the first large-
25 scale field trials of self-healing concrete in the UK testing four different but complementary
26 technologies that were developed. This paper focuses on one self-healing technology, namely
27 microcapsules, which contain a healing agent that is released on their rupture as a result of crack
28 propagation. The paper will present details of the microcapsules used, their implementation in
29 concrete and in the field trials and time-related, field and laboratory, assessment of the self-healing
30 process. It also highlights challenges faced and improvements that are now on-going to produce the
31 next generation of the microcapsule self-healing cementitious system.
32

33 Keywords

34 Self-healing, concrete, site trials, materials for life. microcapsules, applications, construction,
35 materials, testing
36

¹ Present address: Klohn Crippen Berger, Vancouver, BC, V5M 4X6, Canada

² Present address: School of Engineering and Technology, University of Hertfordshire, College Lane Campus, Hatfield, AL10 9AB, UK

37 1 Introduction

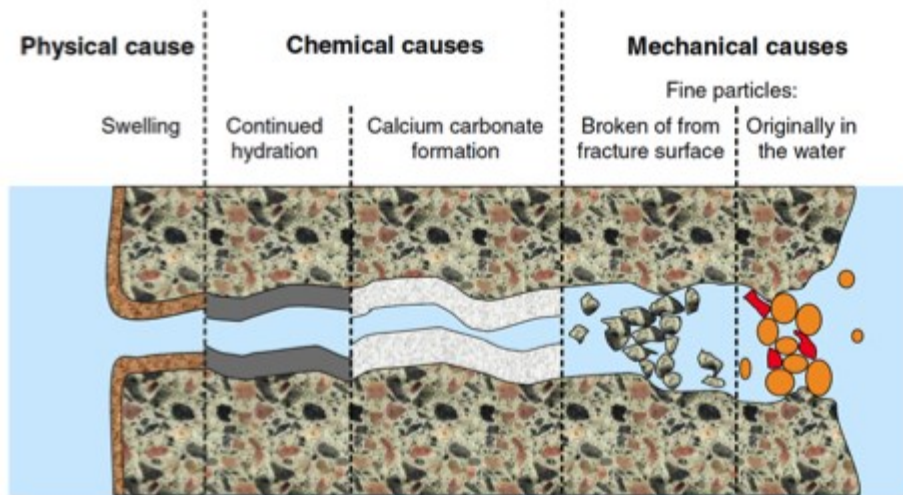
38 1.1 Infrastructure and biomimetic materials

39 Infrastructure assets (e.g. bridges, tunnels, motorways, dams and embankment) are a nation's
40 lifeline and are vital for societal and economic growth. The deteriorating state of the ageing UK
41 infrastructure, and similarly around the world, is the result of decades of underinvestment. The UK
42 recently committed to an investment of £500 Billion in infrastructure by 2020-2021 [1] in valiant
43 efforts to save the nation's infrastructure assets. The majority of infrastructure assets are made out
44 of cementitious composites, mainly concrete. Current figures show that half of the construction
45 budget is spent on the repair and maintenance of mainly concrete infrastructure at around £40
46 Billion/year [2]. Concrete deterioration is the result of traditional civil engineering design practices
47 that are still based on the assignment of appropriate partial material and action factors and
48 providing redundancy to prevent failure. Material degradation is viewed as inevitable and mitigation
49 necessitates expensive inspection, maintenance, repair and replacement regimes. Hence poor
50 material performance continues to be the single main cause of deterioration and failure in our
51 infrastructure systems. Moreover, the durability of repaired concrete structures continues to be
52 major concern as after 5 years, 20% of all repairs fail, increasing to 55% after 10 years [3].

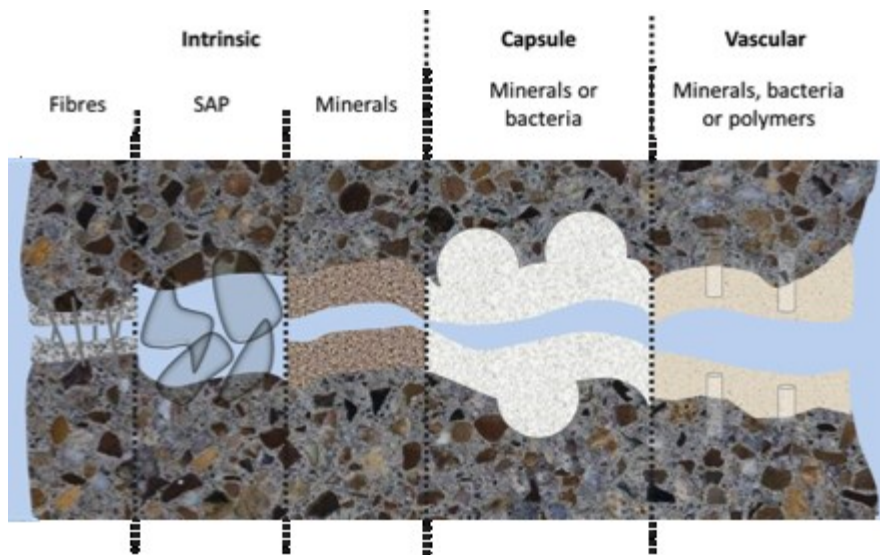
53 While the construction industry is the single largest consumer of resources and raw materials, and
54 accounting for 6% of GDP, it remains the slowest sector to adopt and adapt to new technologies and
55 advanced materials, due to its historic conservative approach to product design and delivery [4].
56 Construction materials have historically suffered from being perceived fundamentally as a cheap and
57 straightforward commodity, where the application of often expensive cutting-edge material
58 technologies is simply not justified. This view can no longer be sustained due to the huge volumes
59 used and associated high carbon footprint as well as the extensive and expensive maintenance
60 regimes that are needed to maintain our infrastructure assets. A new approach to material design
61 through mimicking natural biological systems, in their ability to self-heal, has been adopted in some
62 sectors, with commercial success, through the development of a new class of biomimetic materials.
63 Biomimetic materials are advanced materials that can transform our infrastructure by embedding
64 resilience within its components and systems so that rather than being defined by individual events,
65 they can evolve and adapt over their life span. National and international government and industry
66 road-mapping reports [4–7] have highlighted that advanced infrastructure materials, with specific
67 reference to biomimetic attributes, will play an essential part in the future transition of
68 infrastructure. This will provide a much higher level of confidence in the reliability of the
69 performance of our infrastructure systems but will also require a complete paradigm shift across the
70 design, procurement, construction and maintenance of our infrastructure.

71 In cementitious systems, while different forms of damage result from the wide range of
72 environmental and mechanical actions, cracking is the most widely and commonly encountered. As
73 a result self-healing of cracks in cementitious systems has been widely studied [8,9]. In this context,
74 self-healing phenomena in cementitious systems are broadly classed into two categories: Autogenic
75 and Autonomic (Fig. 1a-b). Autogenic self-healing refers to self-healing processes that are an intrinsic
76 characteristic of the components of the matrix which are usually effective for small crack widths of
77 $\leq 0.15\text{mm}$ and under water curing. Autonomic self-healing refers to actions that use components
78 that do not naturally exist in the cementitious composite, i.e. 'engineered' additions that are usually
79 employed to deal with larger crack sizes and under less favourable curing environments. Some
80 autogenic and autonomic self-healing systems work in combination so that the autonomic system
81 works to reduce the crack size to enable autogenic processes to complete the self-healing process.
82 The work presented in this paper relates to the use of microcapsules for autonomic self-healing in
83 cementitious systems.

84



(a)



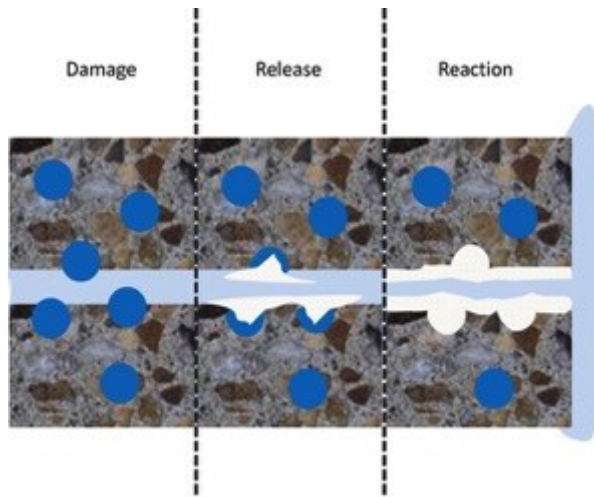
(b)

Figure 1 Self-healing mechanisms for cracks in cementitious systems (a) autogenic self-healing (Reproduced with permission, 2013 Springer [8]) and (b) autonomic self-healing (Reproduced with permission[10]).

1.2 Microcapsule-based systems for self-healing in cementitious systems

Microcapsules are micron-size particles consisting of a stable shell enveloping a cargo, which could be solid, liquid or gases, and serve a wide range of applications in different sectors. They are already in commercial use in construction materials for heat proofing, e.g. phase change materials, and air entraining agents, both incorporated directly into the building material mix composition [11]. Since White et al. [12] introduced the use of microencapsulation for self-healing of polymers in 2001, microencapsulated healing agents for autonomic self-healing has attracted much attention. Embedded microcapsules in materials imbue the ability of a localised response to damage upon rupture, and subsequent release and activation of the healing agent. The proof of concept for microcapsule-based healing in concrete was recently demonstrated [13,14]. The fundamental principle of autonomic self-healing via microencapsulation is that when cracks propagate in the cementitious matrix, they mechanically rupture the dispersed microcapsules and their content (cargo material) is released into the crack volume. Similar to encapsulation, the self-healing mechanism will rely on the nature of the cargo material; namely it may react with an activator (provided as a two-part system e.g. 2-part epoxy system), the cementitious matrix (including

109 hydration and carbonation products e.g. lime) or the environment (e.g. air, moisture for example
110 cyanoacrylates) to form products that fill, seal or heal the crack (Fig. 2). Much of the published
111 literature on microencapsulation-mediated healing has focused on cyanoacrylates or 2-part epoxy
112 for their rapid hardening and high strength, hence quickly providing strength regain. However their
113 high toxicity, high cost and short shelf-life prohibit their use commercially. Recent research has
114 focused on the development of suitable microcapsules taking into consideration parameters
115 affecting the bond strength and boundary conditions to enhance chemical compatibility with the
116 cementitious matrix. Moreover healing agents that can deliver healing products of more compatible
117 nature to the concrete matrix such as encapsulated bacterial spores and mineral cargos including
118 colloidal silica and sodium silicate have recently been considered. A review of the various
119 microcapsules systems can be found elsewhere [9].



120

121 **Figure 2 Schematic of microcapsule mediated self-healing in concrete [10].**

122 A number of experimental procedures have been developed and used to assess the self-healing
123 efficiency in cementitious systems which include quantification of the mechanical recovery (e.g.
124 compressive and flexural strength) using multiple cycles of static loading and reloading or non-
125 destructive measurements as well as permeability measurements [15]. A review of the recent
126 literature, relevant to self-healing microcapsules, shows changes in a variety of material properties
127 when adding microcapsules into cementitious mixes; including workability, permeability, elasticity
128 and strength, although the exact effect is highly dependent on the dosage, size, cargo and particular
129 characteristics of the microcapsules [9].

130 Previous work by the authors confirmed the potential of mineral microencapsulated cargos, in glass
131 tubes, for use in self-healing cementitious materials, with a focus on sodium silicate [16,17] which is
132 commonly used as a repair agent. Different polymeric microencapsulation systems for the sodium
133 silicate were considered [10,18]. The most promising developments included the production of
134 microcapsules with polymeric gelatin/gum Arabic shell, with switchable mechanical properties that
135 ensured the required performance during the mixing and in response to a mechanical trigger [19].
136 The effect of these sodium silicate containing microcapsules was investigated on both the fresh
137 (viscosity, setting time) and hardened properties (modulus of elasticity, compressive and flexural
138 strengths) [19–21]. In these studies, work was also carried out on identifying the healing potential of
139 these microcapsule-based systems under different cracking regimes and degrees of damage. While
140 mineral healing agents do not provide the same level of mechanical strength recovery as its
141 cyanoacrylate counterparts do, they were show to provide significant permeability reduction, hence
142 providing efficient sealing and healing that will prevent ingress of aggressive chemicals and protect
143 against corrosion.

1.3 Large-scale and field application of self-healing concrete

144
145 To date, most of the developments on autonomic self-healing cementitious systems have largely
146 taken place in the laboratory. The first scale-up application of self-healing technologies in concrete
147 was carried out in the 1990s by Dry at the University of Michigan simulated different damage
148 scenarios for bridge elements and pavements in full scale and later field scale trials [22]. Reinforced
149 concrete beams (0.15m x 0.15m x 1.8m) were constructed with embedded continuous brittle glass
150 tubes in their tensile side. Three different healing agents were investigated including a two-part
151 epoxy, cyanoacrylate and a silicon-based adhesive. The reinforced concrete beams were cracked to
152 failure under three-point bending, allowed to recover and then retested to assess the potential for
153 mechanical recovery. Although the reported results were inconsistent as to the performance of the
154 healing technology, some strength regain was possible. Since then, other scale-up work of reinforced
155 concrete samples with embedded glass tubes containing self-healing agents and subjected to cycles
156 of loading and unloading was reported. Thao [23] considered a series of reinforced concrete
157 elements embedded with glass tubes containing an isocyanate prepolymer fastened to their
158 reinforcement bars. A concrete beam (125mm x 200mm x 2000mm), concrete columns (200 x 800mm)
159 and slabs (1000mm x 10000mm x 100mm) were investigated. When the beam was loaded under
160 four-point bending, the embedded tubes showed breakage and subsequent release of the
161 encapsulated agent. Columns were loaded to induce cracking and release of healing agents.
162 Reloading of the column showed the formation of new cracks without any reopening of the
163 previously healed cracks, due to complete recovery of the strength following self-healing. Subjected
164 to impact-loading, the control slab showed a continuous loss in stiffness whilst the self-healing slab
165 showed stiffness recovery up to 99%. Similarly Karaiskos et al [24] also added glass-encapsulated
166 healing agents (polyurethane) into a 150mm x 250mm x 3000mm reinforced concrete beam. 350
167 glass tubes each 50mm in length were added 10mm from the base of the beam by attaching them to
168 a plastic grid. Cracks were induced by loading the beam in four-point bending until the average
169 measured crack width reached 0.25mm. Beams were then reloaded after a seven-week healing
170 period and several non-destructive testing (NDT) methods were used to monitor healing of cracks.
171 These included ultrasonic pulse velocity, piezoelectric transducers, acoustic emission and digital
172 image correlation. Results were compared with a control beam without the glass tubes. No
173 significant recovery in mechanical properties was observed for either beam although the use of a
174 variety of NDT methods proved useful for monitoring crack formation, propagation and closure.

175 Transfer of developed self-healing technologies from larger laboratory-scale experiments to field-
176 scale structures has been limited. In addition to overcoming practical challenges of up-scaling the
177 healing technology, the in-situ application of any self-healing approach possesses unique challenges
178 and obstacles. Field scale reinforced concrete applications of capsule-based self-healing concrete
179 have been implemented [25,26]. Full scale reinforced concrete bridge decks (7m x 1.2m x 0.075m)
180 were constructed, embedded with discrete glass fibres (100µm) containing a combination of
181 sealant/adhesives. Brittle fibres placed close to the surface of the bridge deck targeted transverse
182 shrinkage cracking. After one month, the fibres were seen to break releasing the sealant creating a
183 controlled expansive joint. The efficiency of the healing mechanism under mechanical damage was
184 also investigated. Load-induced cracks were generated using a pneumatic jack at mid-span causing
185 the glass fibres to break and release the adhesive into the cracks. Subsequent reloading of the
186 bridge deck was also conducted to test the efficiency of the adhesive in the regain of mechanical
187 performance. Increased strength regain was demonstrated compared to a control deck with new
188 cracks opening during reloading before the original cracks reopened. Re-release of repair adhesives
189 in second and third loadings occurred in all of the decks containing repair adhesives showing good
190 long-term survivability of the encapsulated healing agent. A few large scale field applications of
191 bacteria-based self-healing concrete have also been realised [27,28]. Here, bacteria were added into
192 the concrete mix that metabolise added calcium lactate to produce calcium carbonate. The first field
193 application involved 3m-long concrete linings for an irrigation canal in Equador containing LWAs
194 impregnated with alkaliphilic spore-forming bacteria [29]. After five months, the cast concrete

195 showed no sign of cracking or deterioration and therefore its healing performance could not be
196 evaluated. Researchers at Delft University of Technology were first to implement self-healing
197 concrete in a building[28]. A lifeguard station consisting of bacteria-based concrete has also been
198 built [30]. However, no publication of results of how the building is performing to date could be
199 obtained.

200 A national UK team, from the universities of Cambridge, Cardiff and Bath, has come together,
201 through research council funding, to develop the first generation of self-healing cementitious
202 systems in the UK to address cracks across many length scales [31–33]. This led to the development
203 of a suit of complementary technologies namely microcapsules, calcite precipitation bacteria, shape
204 memory polymer tendons and vascular networks (Fig 1b). These can be used in isolation or in
205 combination depending on the nature and extent of the damage. Extensive system development
206 and material testing was carried out in the laboratory. Collaboration with industry partners led to
207 scaling up of the technologies and to the first UK full-scale field trials of the developed system in
208 concrete retaining wall panels, on the Welsh Government A465 Heads of the Valleys Upgrade
209 scheme project. Five concrete panels were cast- each being 1.8m tall, 1m wide and 150mm thick
210 (shown in Fig. 3). Details of the design and execution of the field trials were presented elsewhere
211 [34,35]. One of the panels contained the developed microcapsules and there was a control panel
212 without any microcapsules with which a comparison was made. This paper focuses on the former. It
213 presents details of the scaling up of the microcapsules and their use in the field trials and
214 subsequent performance and monitoring.



215
216 **Figure 3 Self-healing concrete wall panels constructed within the EPSRC and industry funded**
217 **Materials for Life (M4L) project [35].**

218 2 Materials and Testing

219 2.1 Microcapsules and concrete mixes

220 The microcapsules used here were the result of industrial collaboration, which led to the design and
221 production, using complex coaccervation, of gelatin/gum Arabic shell microcapsules containing
222 sodium silicate (SS) as the cargo [19]. The sodium silicate was in an emulsion with mineral oil and
223 emulsifier and formed ~42% of the cargo. The microcapsules (seen in Fig. 4a) had a mean diameter
224 of 290 μm with a standard deviation of ~120 μm and were provided in a preserving solution (Fig. 4b).
225 The microcapsules had switchable mechanical properties such that they initially had ductile
226 ‘rubbery’ behaviour, which guaranteed their survivability during concrete mixing, and then became
227 brittle, and easy to fracture, in the set concrete as water was removed from the shell [19]. Based on
228 the results from related laboratory studies on the effect of the microcapsules on the fresh and
229 hardened material properties and healing potential of mortars [21] and concrete [36], 8%
230 microcapsule content by volume of cement (v_v) was selected for application in the field trials. This
231 dosage was found to provide an optimum level of healing, showed high compatibility with the
232 mortar matrix and had negligible effects on the workability, setting time and strength development.

233 The concrete mix composition is detailed in Table 1. The microcapsules were first washed with water
 234 and filtered from their preserving solution before being added, in their slurry form, directly into the
 235 ready-mix C40/50 concrete using a portable 120L Belle concrete mixer. The microcapsules were
 236 added at 8% by volume of the cement, corresponding to $\sim 2.67\%$ by weight of the cement and
 237 $\sim 0.47\%$ of the total concrete mix. A small quantity of water was used to wash out the microcapsules
 238 from the container and as a result the effective water-to-cement (w/c) ratio of the concrete mix
 239 increased from ~ 0.43 to ~ 0.45 . A control panel was also cast without any microcapsules.



(a)

(b)

Figure 4 The microcapsules used in the field trials; (a) the microcapsules under the microscope [19] and (b) microcapsule slurry as delivered to site [35].

240

241
 242
 243 **Table 1** Composition by % weight of the ready mix C40/50 concrete (supplied by Hanson UK) and
 244 the microcapsules used in the site trial.

Material	Quantity for field trials (kg/m ³ unless noted otherwise)
Cement (CEM I)	415
10mm Limestone aggregates	944
Limestone fines (0-2mm)	396
Marine sand	393
Water	179 (w/c 0.43)
Admix: Plasticiser	0.35 L/100kg cement
Admix: Retarder	0.1 L/100kg cement
Microcapsules (slurry)	11.1

245

246
 247
 248 **2.2 Crack initiation and monitoring**

249 The wall panels were designed to crack 500mm from the base upon loading, which was facilitated by
 250 using 16mm diameter starter bars on the front face up to the designed crack location, before
 251 changing to the 10mm diameter mesh to create a weak section in the panel as seen in Fig. 5. Loading
 252 was applied using a hydraulic jack positioned 1.5m above the base of the panels, i.e. near the top of
 253 the wall, that was used to pull a threaded bar; thereby inducing a cantilever load. A wailing beam
 254 attached to the front of the panel allowed a distribution of load across the width of the wall. Full
 255 details of the design and construction of the walls is given elsewhere [35]. Panels were painted with
 256 a black-and-white speckle pattern for digital image correlation (DIC) analysis to monitor wall
 257 displacements and associated strains that arise during loading and unloading (Fig. 6).
 258

259 Prior to loading, air permeability measurements at various locations around the wall face were taken
 260 as initial reference measurements using a field permeability tester [37], particularly in the region
 261 where cracking was expected to occur (Fig. 7). The permeability of the concrete cover (that between
 262 the steel reinforcement and external environment) must be sufficiently sound as an indicator of

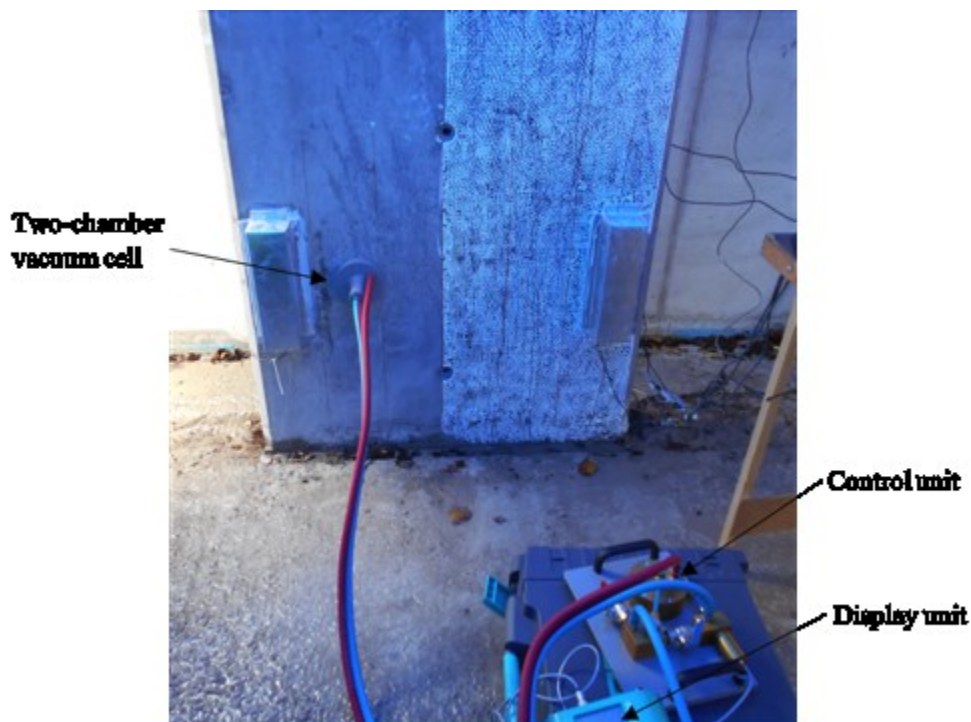
263 good durability. Air permeability testing allows a non-destructive measurement of the quality of the
264 concrete cover on site and involves applying a vacuum inside a cell placed on the concrete surface
265 and then measuring the rate at which the pressure returns to the atmospheric value. The two-
266 chamber vacuum cell is connected to a pressure regulator that balances the pressure in the inner
267 (measuring) chamber and in the outer (guard-ring) chamber. Data was collected automatically by
268 the display unit and the permeability coefficient (kT) and the depth of penetration (L) of the vacuum
269 was calculated. The air permeability measurements are generally in good agreement with laboratory
270 methods [37] and the testing equipment adheres to SN 505 252/1, Annex E.



271
272 **Figure 5 Wall panel reinforcement design to ensure cracking at ~500mm from the base of the wall**
273 **panel.**



274
 275 **Figure 6** The microcapsule wall panel half painted with a black-and-white speckle pattern for DIC
 276 analysis

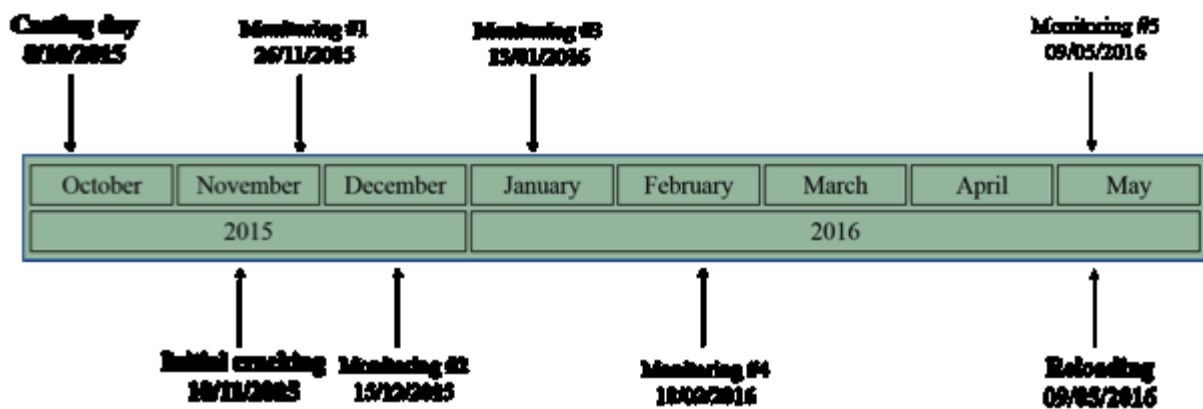


277
 278 **Figure 7** Air-permeability testing device obtaining measurements around the expected crack
 279 generation area.

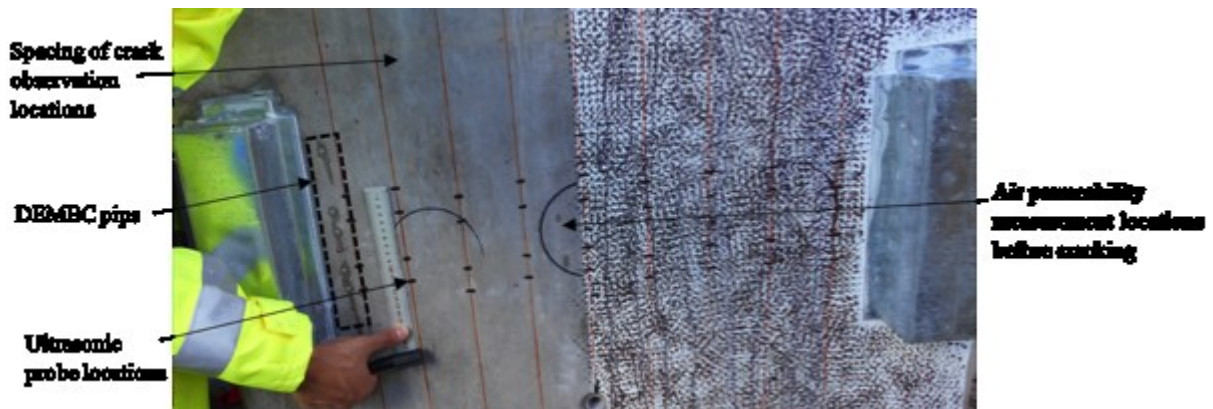
280

281 A timeline of the field trials experimental programme is given in Fig. 8. The wall panels were initially
 282 loaded 5 weeks after their casting day and then reloaded after a 26-week healing period. Loading
 283 was applied until a noticeable crack appeared at the designed height and a large drop-off in load was

284 observed. After the healing and monitoring period, the walls were reloaded to the residual (drop-
 285 off) load. Four linear variable differential transformers (LVDTs) were used to measure lateral wall
 286 displacements. The LVDTs were located at the same height as the load application: two recording
 287 displacements of the wall panel and two recording displacements of the reaction wall. A mean of the
 288 lateral wall displacement was used when plotting load-displacement curves. A further two LVDTs
 289 were used to record crack opening by mounting them vertically on the front of the wall panel,
 290 ensuring that they span across the expected location of induced crack. Demountable mechanical
 291 strain gauge (DEMEC) pips were attached adjacent to the LVDTs to measure crack opening (Fig. 9).
 292 Once the panels were cracked, the load was kept constant and DEMEC measurements were taken.
 293 To complement the latter, microscope images were taken along the crack length spanning the panel
 294 width using a handheld digital microscope. After the acquisition of DEMEC measurements and
 295 microscope images, the load was gradually released from the wall panel. After complete unloading,
 296 DEMEC measurements and microscope images were taken once again, at the same exact points, to
 297 measure the residual crack width.



298 Figure 8 Timeline of wall panels testing and measurement collection dates
 299



300 Figure 9 Location of DEMEC pips, ultrasonic probe measurement locations and air permeability
 301 measurement locations.
 302

303

304 The DIC software measured displacements through the comparison of images to monitor movement
 305 in the speckle pattern. Photographs of the wall were taken at each kN load applied (or released)
 306 using two digital cameras and flash equipment set up on a tripod facing the wall panel (Fig. 10). The
 307 use of DIC allowed monitoring of crack initiation, coalescence and propagation. The covering of one-
 308 half of the wall face only in the speckle pattern offset any potential variations in obtained
 309 measurements due to the hydrophobic/water repellent nature of the paint. After initial cracking, a
 310 strip of thermal insulation foil roll was placed across the middle section the microcapsule wall to
 311 reduce its exposure to the environment. This was to examine the effect of sealing on the overall
 312 healing progress for both halves of the wall although the insulation was permanently removed after

313 Monitoring event #1. Weather data was collected from local weather stations in Tredgar and Usk
314 between October 2015 and May 2016 including daily minimum air temperature, maximum air
315 temperature and total rainfall.



316
317 **Figure 10 Digital Image Correlation camera and tripod set-up on the microcapsule wall.**

318

319 Between initial cracking and reloading stages, various measurements were periodically taken from
320 the wall panels to assess crack closure and monitor self-healing. Microscope images were taken
321 from at least five observation locations along the crack length. Using this data, interpolation of crack
322 width along the crack length was carried out allowing a visual representation of crack width across
323 the wall panel throughout the healing period. Crack width healing values were also calculated in
324 order to quantify crack closure. The crack width healing percentage compares measured crack width
325 values with the initial crack opening at that point following cracking and load-release. Crack width
326 healing (*CWH*) was calculated as shown in Equation 1:

$$CWH = \frac{w_i - w_h}{w_i} \times 100\% \quad (\text{Eq. 1})$$

327

328 where w_i is the initial crack width and w_h is the healed crack width.

329 Visual observations on the specimen surface only provide an indication of the extent of self-healing
330 occurring at the crack mouth and do not provide insight into the healing processes that take place
331 deeper into the crack. Therefore, non-destructive techniques such as the use of ultrasonic wave
332 transmission and air permeability were used to provide information about internal densification and
333 self-healing. An ultrasonic pulse velocity test instrument complying with European standard
334 EN12504-4 and BS1881:Part 203 was used to measure the crack depth at each of the crack
335 observation locations during the monitoring events. The ultrasonic probes were placed on the
336 concrete surface adjacent to the crack and ultrasonic couplant was used between the surfaces to
337 facilitate transmission. Water-saturation of the walls hindered both the ultrasonic and air
338 permeability measurements throughout the monitoring period. Subsequently, only three monitoring
339 events were possible for the former; namely after cracking, at 2 weeks and at 26 weeks (monitoring
340 #1 and #5 respectively) whereas only two for the latter; after cracking and at 26 weeks (monitoring

341 #5). This was due to the consistently high levels of rainfall in the area particularly over the wet
342 winter months.

343 2.3 Microstructural analysis

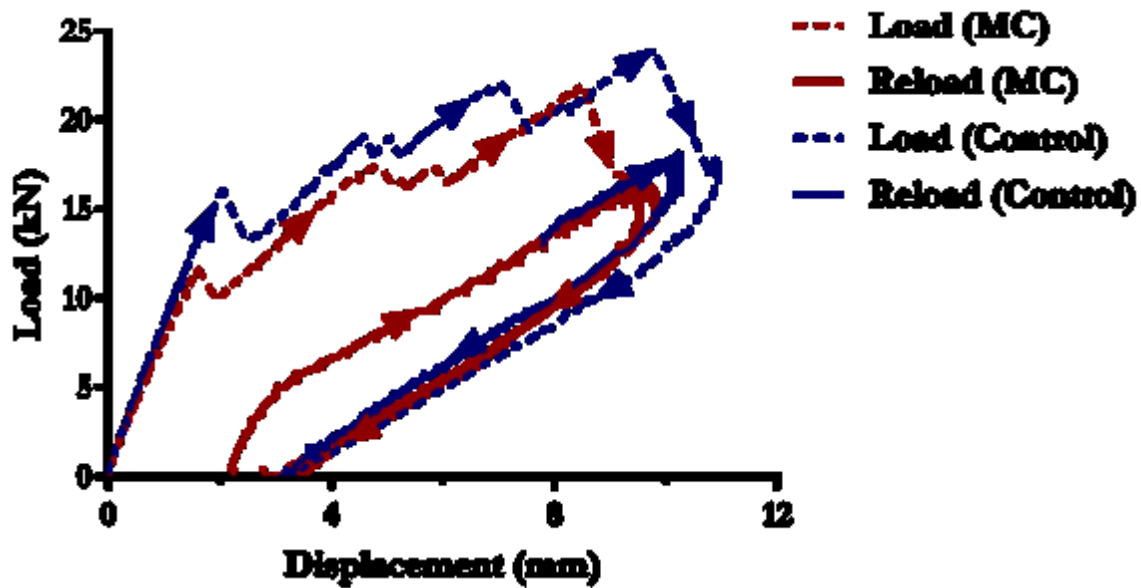
344 Following the re-loading of the wall panels, hence at 6 months, material was extracted from the
345 crack surface after load removal. A multi-tool fitted with a grout removal attachment was used to
346 carve our pieces of materials extract and also powder that was later passed through a 40 μ m sieve
347 for laboratory investigations of the microstructure to quantify the products that formed in the
348 cracks. Tests employed include scanning electron microscopy (SEM), X-ray Diffraction (XRD),
349 thermogravimetric analysis (TGA) and differential thermogravimetric analysis (DTG). In addition,
350 cores 100 mm in diameter and 200 mm high were also cored from the microcapsule wall and tested
351 in a CT scanner to observe the homogeneity of the distribution of the microcapsules within the
352 concrete and how intact they are.

353 3 Results and Discussion

354 3.1 Characteristic strength and mechanical loading

355 The characteristic cube strength obtained of the concrete mixes tested at 28 days without and with
356 microcapsules were 59.3MPa \pm 0.85 and 42.2MPa \pm 3.8 respectively. Although previous lab work
357 [36] had indicated that the addition of microcapsules would have a minimal effect on the strength of
358 the concrete the observed values suggested a strong effect on strength development. It was
359 stipulated that the great variation and discrepancy in results for cube strength for the site mixes is
360 the result of significantly deteriorated workability and honeycombing. The reason for this being the
361 double handling of the concrete to enable the microcapsules to be added to the mix as well as
362 inadequate hand compaction of the cube specimen as a consequence of the casting sequence
363 adopted on site.

364 The load-displacement relationship for both panels for initial loading and reloading seen in Fig. 12
365 confirm that the strength of the panel as not compromised by the addition of the microcapsules.
366 This figure shows that both the initial peak loads obtained, 23.9kN and 21.9kN for the control and
367 microcapsule panels respectively, and the residual loads, 17.4kN and 16.2kN respectively, suggest a
368 smaller decrease (\sim 8%) due to the presence of the microcapsules. Similarly, the concrete stiffness
369 values were also seen to only decrease by \sim 8% from 7.8kN/mm in the control panel to 7.1kN/mm in
370 the microcapsule panel. These results are in better agreement with the cylindrical compressive
371 strength results for microcapsule-loaded concrete samples cast and tested in the laboratory (\sim 9%)
372 [36] as well as previous laboratory observations for mortars [21].

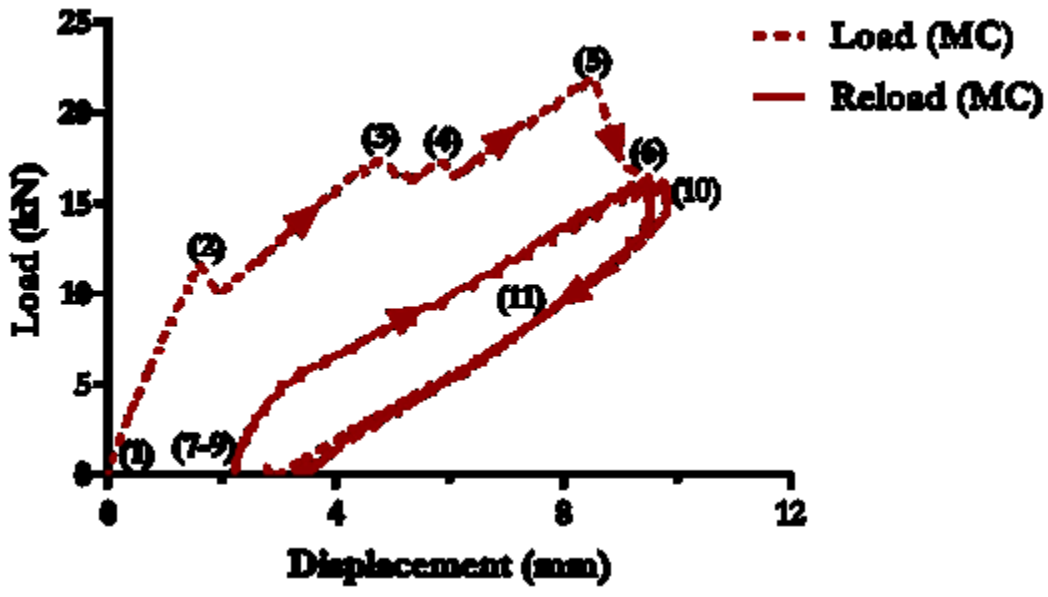


373

374 **Figure 11 Initial and reload load-displacement curves for the microcapsule and Control wall panels.**

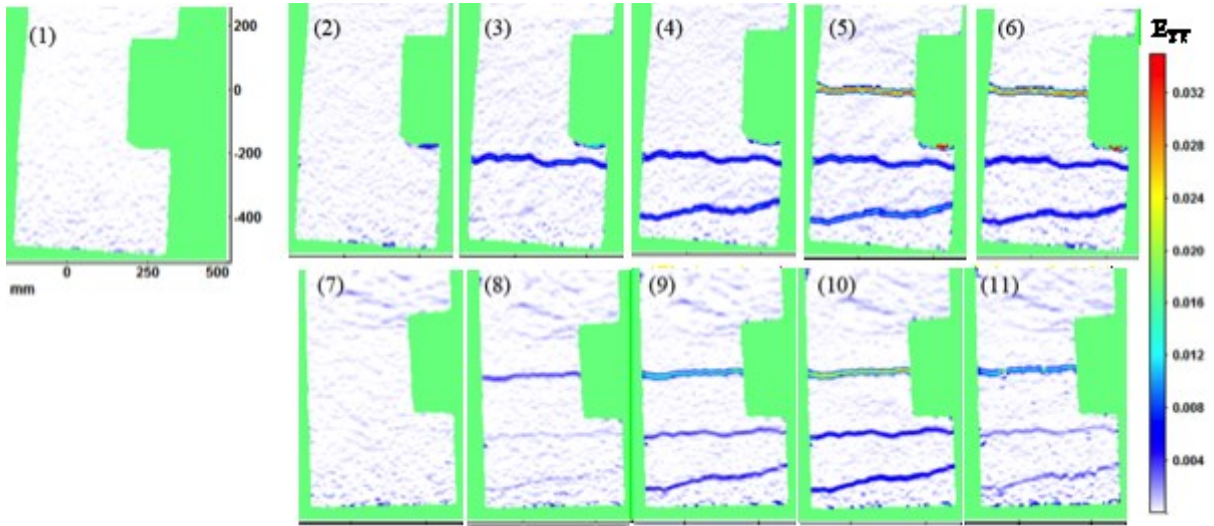
375 Several microcracks were formed during loading, evident from the various drops in the load-
 376 load-displacement curves (Fig. 12a and 13a). The first crack was noticed at 16.1kN (~72% of maximum
 377 load) and 11.6kN (~55% of maximum load) in the control and microcapsule walls respectively. This
 378 microcracking was also clearly visualised in the DIC images showing vertical strain E_v , since loading
 379 induced tensile stresses normal to the plane of the crack (i.e. mode I crack separation). In the
 380 microcapsule panel, a microcrack formed at ~280-300 mm from the base before a second
 381 microcrack formed below this at between 30-100mm (Fig. 12b). In comparison, for the control
 382 panel, a microcrack first formed closer to the base at 50-100mm and then a second between 200-
 383 250mm (Fig. 13b). Despite those differences, two significant microcracks were formed in both walls
 384 between the designed crack location and the wall's joint with the base slab. The third crack was then
 385 generated at the designed location 500mm from the base, resulting in failure of the wall. Due to
 386 technical logging issues, the initial reload curve for the control panel was not obtained.

387 The DIC results show that during reloading it was the main crack that first re-opened before the
 388 opening of the other two microcracks occurred in both the microcapsule (Fig. 12b) and control wall
 389 (Fig. 13b), confirming that low strength regain is possible by autogenic healing or mineral based-
 390 autonomic healing. This is in agreement with previous unconfined compressive strength (UCS) and
 391 flexural laboratory tests on the microcapsule-based concrete system [36] where an addition of 8%
 392 microcapsules achieved 10% more strength than the control and an absolute strength recovery of
 393 25% over the monitored period.



394
395
396

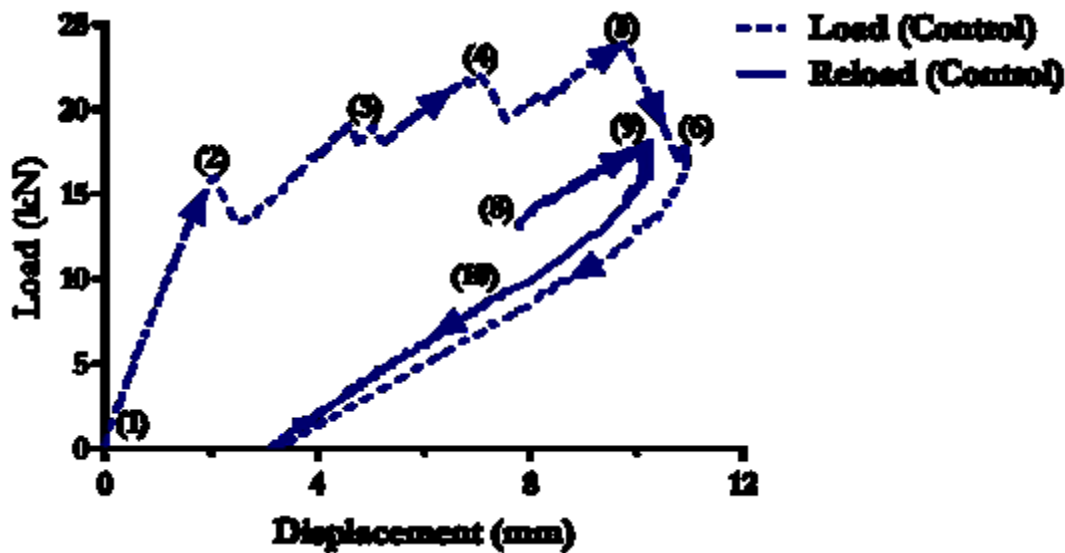
(a)



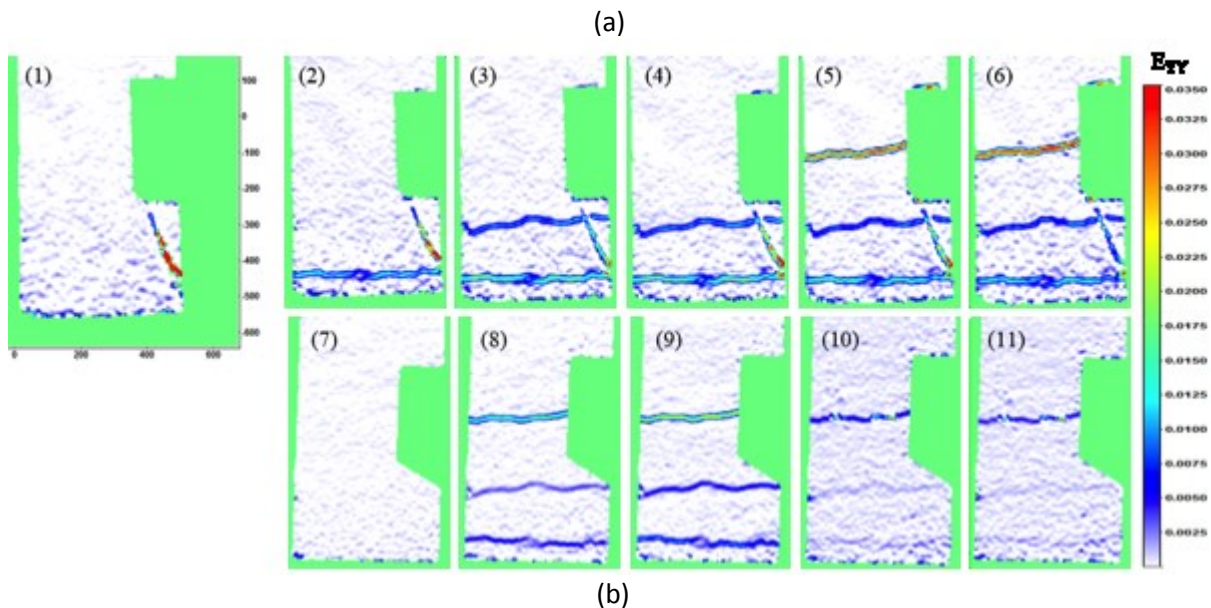
(b)

397
398
399
400

Figure 12 (a) Loading and reloading of the microcapsule wall and (b) corresponding DIC images.



401
402



403
404

405 **Figure 13 (a) Loading and reloading of control wall and (b) corresponding DIC images.**

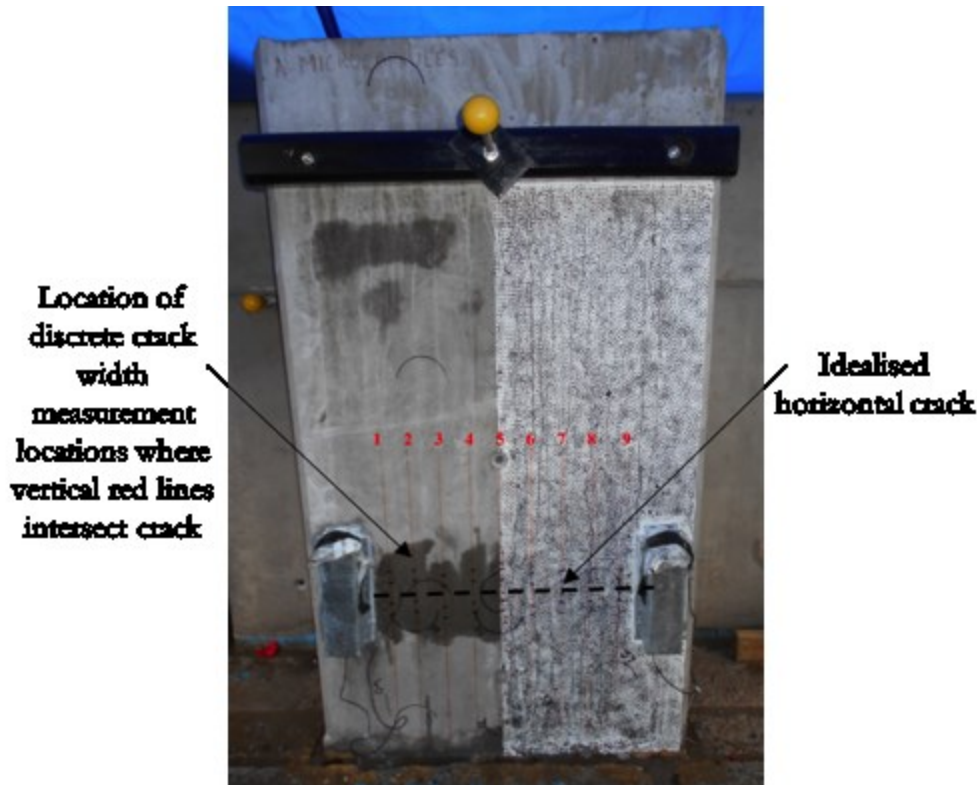
406

407 3.2 Microscopic crack healing

408 Following initial cracking and subsequent load release, residual crack width measurements were
 409 recorded from optical microscope images showing initial average crack widths of 165 μ m and 115 μ m
 410 in the control and microcapsule panels respectively, consistent with the lower load reached in the
 411 latter. The DEMEC and LVDT crack opening measurements results were comparable with those
 412 measured from the microscope images. The progress of healing was monitored throughout the 6-
 413 month testing period through microscope imaging of the crack width. During this monitoring period,
 414 no reduction in DEMEC and LVDT measurements was observed indicating that any reduction in crack
 415 width obtained is not from mechanical re-joining of the crack faces but rather due to the expected
 416 healing mechanism of depositions, filling and sealing within the crack.

417 Interpolation of crack width measurements on different locations along the crack length (shown in
 418 Fig. 14a) can be seen in Fig. 14b in which the colour-bar indicates the level of crack closure achieved.
 419 Similar crack width healing characteristics are seen in both panels with less healing observed on the
 420 right-hand side of wall panel due to the paint required for the DIC speckle pattern. The paint has a
 421 waterproof characteristic and therefore water runs off the surface rather than permeating into the

422 crack and contributing to clogging of the crack mouth. Accelerated average crack healing along the
 423 main crack location, of 49% and 63% was evident as early as monitoring events #1 (14 days) and #2
 424 (28 days) for the MC panel compared to 14% and 36% respectively, observed in the Control panel.
 425 These results not only confirmed preliminary investigation for mortars specimen [21] but also were
 426 in good agreement with microscopic crack width healing reported in laboratory concrete samples
 427 prepared with equivalent microcapsule content. The average crack width healing for cube, cylinder
 428 and prism concrete specimens after a 28-day water-immersed healing period was established in
 429 laboratory conditions prior to the field trials. There, microcapsule-containing samples showed
 430 superior crack closure- reaching ~50%, compared to the control samples with an average of less than
 431 23% [36]. The large variations in areal healing observed in the control laboratory samples were also
 432 consistent with those observed for the Control panel on site.

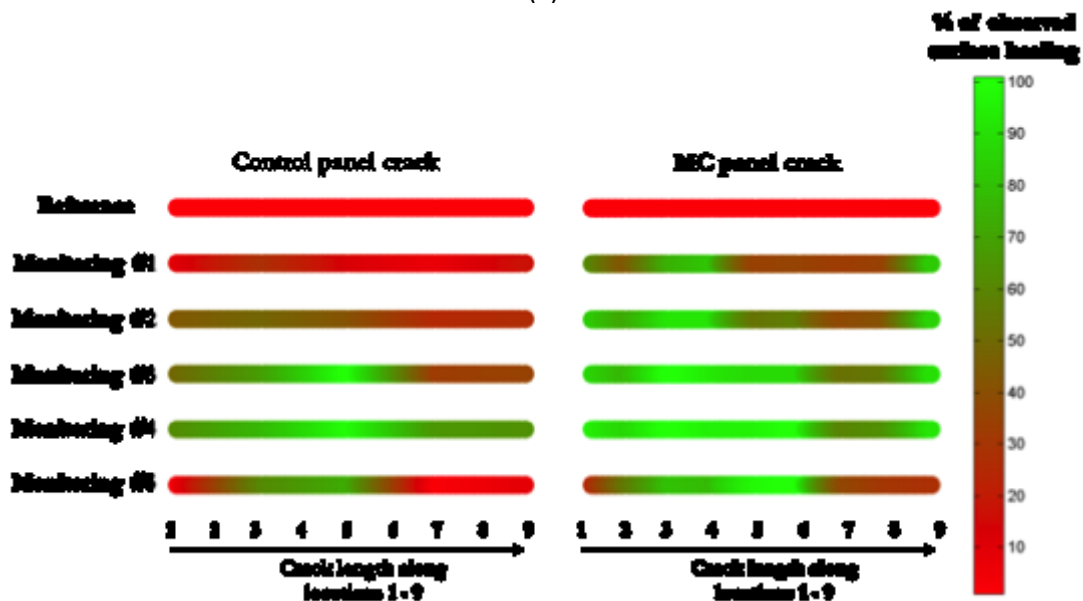


Location of discrete crack width measurement locations where vertical red lines intersect crack

Idealised horizontal crack

433
434

(a)



435

436
437
438
439
440

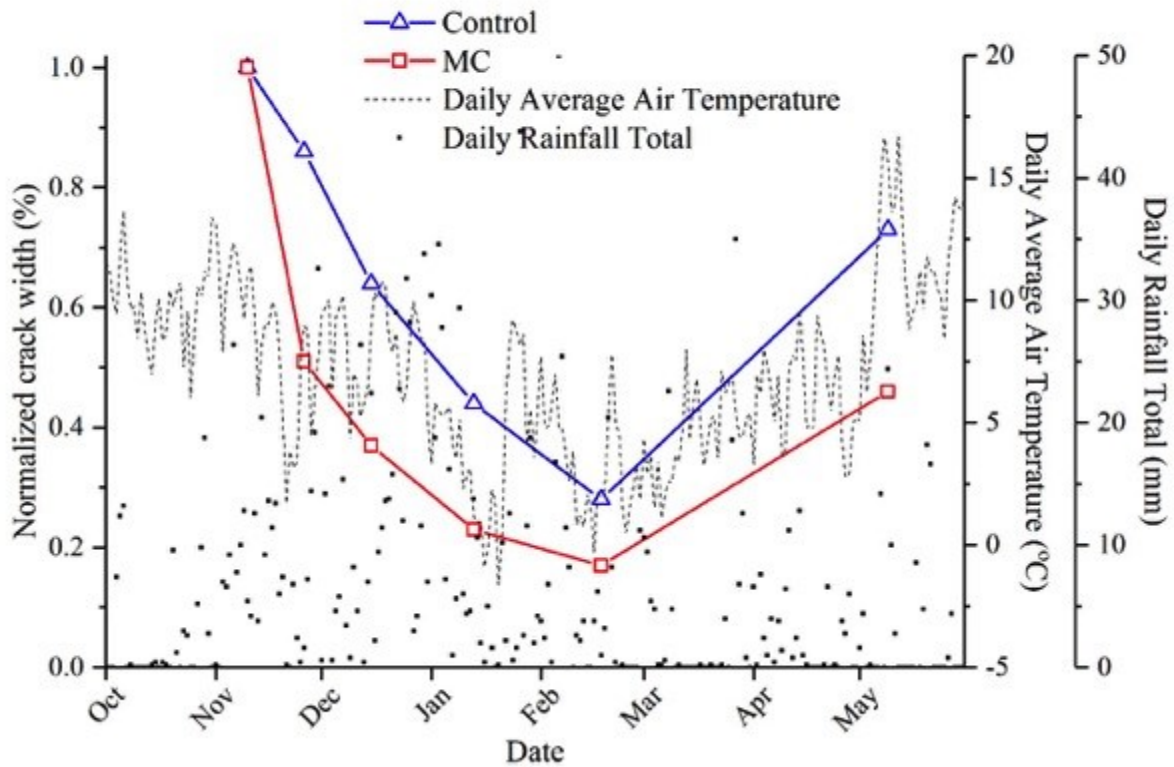
(b)

Figure 14 Monitoring crack width healing in panels: (a) microcapsules wall panel showing the locations (numbered 1-9) at which discrete crack width measurements were taken and (b) continuous crack width healing percentage plots for both panels.

441 Although the observed overall healing was within the expected range with final observed healing of
442 54% and 27% for microcapsule and control wall respectively, a temporal variation of the healing
443 progression between monitoring events was observed in both panels. There is a clear increase in
444 crack opening between monitoring event #4 and #5 for both panels although this is less prominent
445 for the microcapsule wall. Thermal expansion and contraction due to changes in atmospheric
446 temperature contributed to the change in crack width measurements. The mean crack width
447 obtained over the monitoring period can be seen in Fig. 15a along with the daily average air
448 temperature obtained from local weather stations. Crack width measurements are normalised with
449 respect to the width obtained following load removal (i.e. residual crack widths). A trend is clearly
450 observed between the daily average air temperature and the normalised crack width in both the
451 microcapsule and control panels. Crack width measurements constantly reduced during the first four
452 monitoring events (between November 2015 and February 2016). However, the normalised crack
453 width increased for the final monitoring event before reloading of the panels in May 2016 although
454 the measured width is still less than the residual crack width measured upon initial loading of both
455 panels. This indicates that variations in measured crack width cannot be solely due to thermal
456 expansion and contraction but also due to self-healing contributions.

457 The crack in the microcapsule wall shows consistently greater closure than in the control wall
458 throughout the monitoring period. In particular, the initial crack closure (indicated by the negative
459 slope between the first and second measurements) is higher for the microcapsule panel. This
460 indicates that the autonomic self-healing reactions have begun within the first two weeks after
461 cracking. Studies that have explored the efficacy of sodium silicate as a healing agent have observed
462 mechanical binding of sodium silicate with hardened cement paste [16,38] even within 48 hours
463 [39]. It is no surprise therefore, that the autonomic self-healing benefit is realised within the first
464 two weeks of cracking. Since temperatures did fall below 0°C in January and February, freeze-thaw
465 damage may also have contributed to the observed behaviour. Free water that freezes within the
466 concrete pores expands and exerts internal stresses to the material. These stresses may drive open
467 pre-existing microcracks (thereby increasing the observed crack width) or may create new cracks in
468 the material. Cycles of freeze-thaw can cause progressive and cumulative damage.

469 Observations of daily rainfall totals also suggest the contribution of rainwater to the healing process.
470 Fig 15b shows the average normalised crack width along with daily rainfall totals. The greatest
471 amount of rainfall is observed during the first three months after initial cracking; namely in
472 December, January and February. Water is necessary for the reaction of the released sodium silicate
473 with the hardened cement matrix. Furthermore, the presence of water is one of the most important
474 criteria for successful autogenic self-healing [40,41]. The temporary addition of insulation to the
475 microcapsule panel in the first two weeks of monitoring did not appear to have affected the obtained
476 results. Theoretically, less self-healing is expected in the locations that were covered due to water
477 deprivation in the cracks limiting both autogenic and autonomic self-healing processes. However, in
478 this wet environment, the insulation tape was inadequate to provide protection from rainwater and
479 the concrete quickly saturated under rainy conditions.



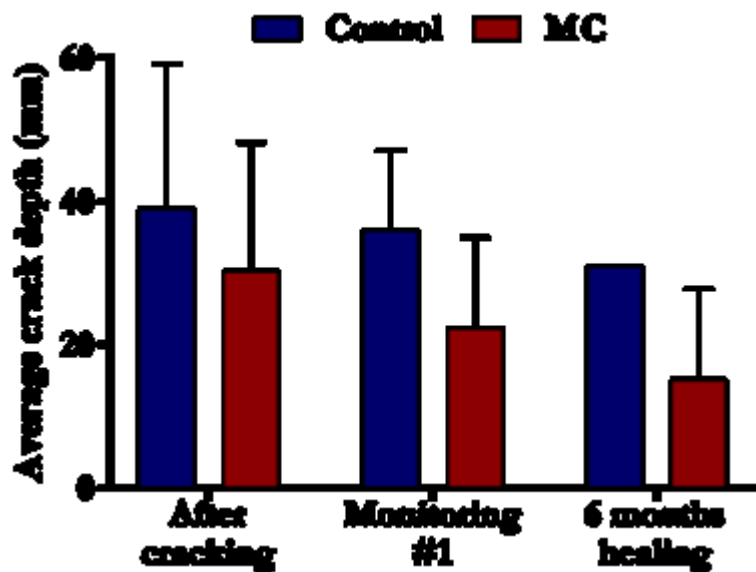
480

481 **Figure 15 Monitoring crack width healing in panels: (a) microcapsules wall panel showing the**
 482 **locations (numbered 1-9) at which discrete crack width measurements were taken and (b)**
 483 **continuous crack width healing percentage plots for both panels.**

484

485 3.3 Crack depth and permeability

486 The crack depth measurements taken with the ultrasonic device on site are presented in Fig.
 487 16. Only three monitoring events were possible; after cracking, after 2 weeks and after 26 weeks
 488 (monitoring #1 and #5 respectively) due to a number of challenges faced with the testing on site,
 489 since measurements were unreliable when the surface of the concrete was wet. In addition, the
 490 uneven wall surface made the use of probes quite problematic. The average crack depth reduced by
 491 ~8% and ~39% after 2 weeks (#1) and ~20% and ~58% after 26 weeks of healing (#5), in the control
 492 and microcapsule walls respectively. Interestingly, the observed relative improvement by the
 493 addition of microcapsules is higher compared to laboratory measurements (~28%) on concrete
 494 samples produced with the same dosage of microcapsules.



495

496

497

Figure 16 Average ultrasonic crack depth measurements after cracking, after 2 weeks and after a 6-month healing period.

498

499

500

501

502

503

504

505

506

507

508

509

510

511

512

513

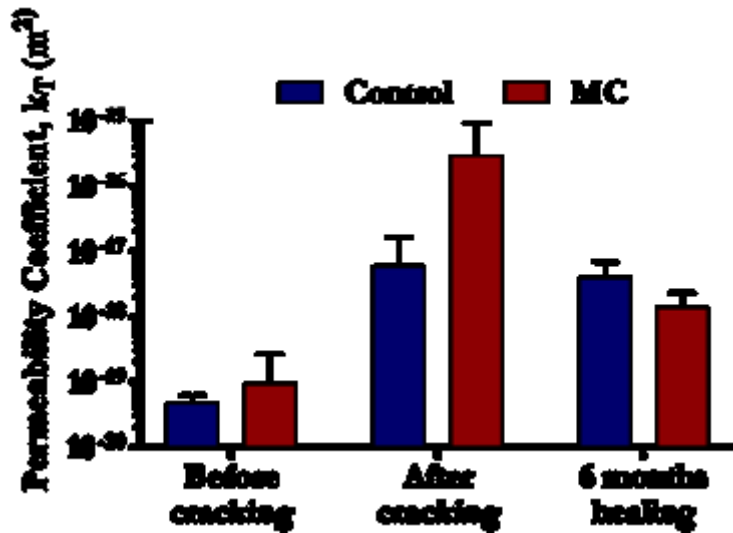
514

515

516

517

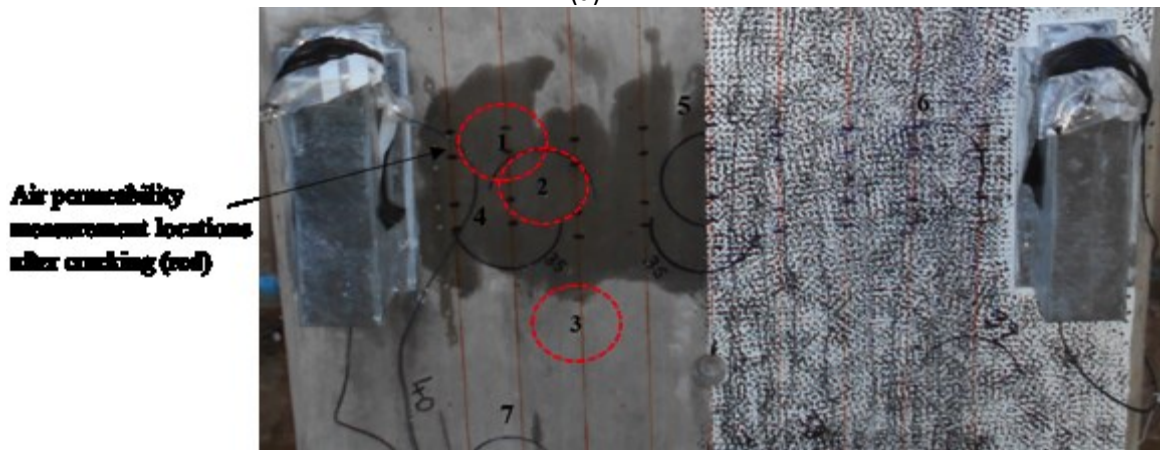
The coefficient of air permeability values measured at three periods are shown in Fig. 17a, showing very similar values of $\sim 10^{-19}$ kT for both walls before cracking suggesting that the microcapsules did not significantly alter the initial porosity of the concrete. This value is typical for concrete of very low permeability [42]. After cracking, the air permeability of the microcapsule wall was noticeably greater than the control wall by ~ 2 orders of magnitude. Since the microcapsule wall failed at $\sim 8\%$ lower load than the control panel and hence slightly weaker, it is possible that this had induced a greater content of internal microscale damage and cracking. It should be noted here, that it was not possible to obtain air permeability measurements after cracking from all of the same locations prior to cracking. When placing the device in locations directly over the induced crack, the device was unable to create a vacuum and therefore obtain a reasonable measurement. Since the crack passed through the initial measurement locations, new locations adjacent to previous measurement locations were chosen (Fig. 17b). At monitoring stage #5 (6 months of healing), the permeability of the control panel reduced only slightly, while that for the microcapsule wall recovered significantly, by >2.5 orders of magnitude, to $\sim 10^{-18}$ kT. The permeability of the microcapsule wall was half an order of magnitude less than the control wall and was consistent with trends observed in the laboratory using sorptivity tests. The average sorptivity coefficients calculated across control and microcapsule-containing concrete samples after a 28-day healing period show that the rate of water absorption by microcapsule loaded samples is generally lower than that of the control [36]. Nonetheless the permeability of both walls remained greater than the permeability prior to cracking indicating only partial self-healing at that stage.



518

519

(a)



(b)

Figure 17 (a) Permeability of wall panels before cracking, after cracking and after a 6-month healing period and (b) Air permeability measurement locations after loading and subsequent cracking of concrete wall panel.

520

521

522

523

524

525

3.4 Microstructural analysis

526

527

528

529

530

531

532

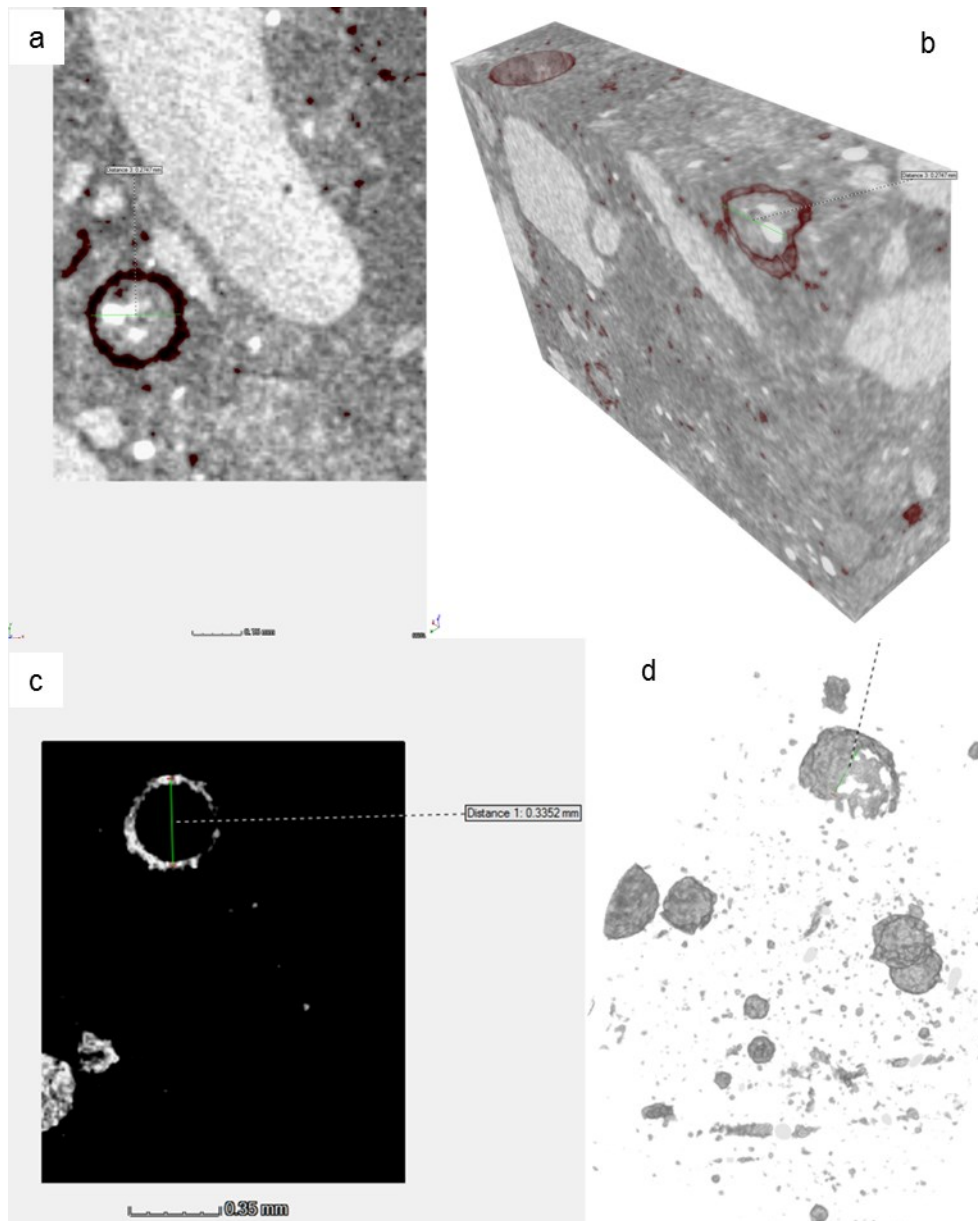
533

534

535

536

Extracted cores were placed in a CT scanner and a typical image is shown in Figure 18. The figure and a detailed assessment of the CT scan images throughout the sample, confirmed uniform distribution of the microcapsules and their intact nature. The shell material was associated with a circular shaped low density material filled with a solid material, as shown in Fig. 18. The circular shape was typically $\sim 250\text{-}350\ \mu\text{m}$, similar size to the microcapsules. As the material is filled with a solid, and not air, we believe that the microcapsules have maintained their functionality yet the core material initially liquid, may have solidified in the time of investigation. Namely the osmotic difference has attracted gradually the water molecules outside of the shell wall to the surrounding matrix. Hence the solid/crystalline sodium silicate (the healing agent) is still within the microcapsules but not in its original liquid state.



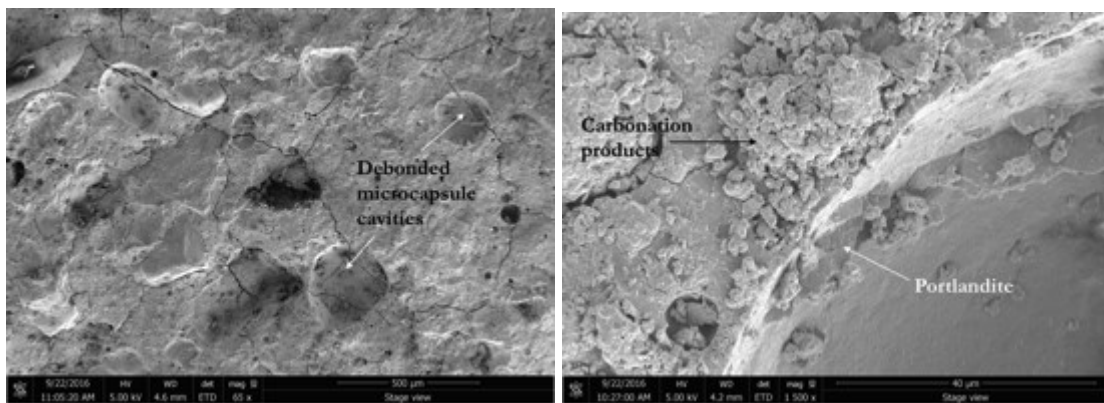
537

538 **Figure 18** μ CT scan image of a core from the microcapsule wall.

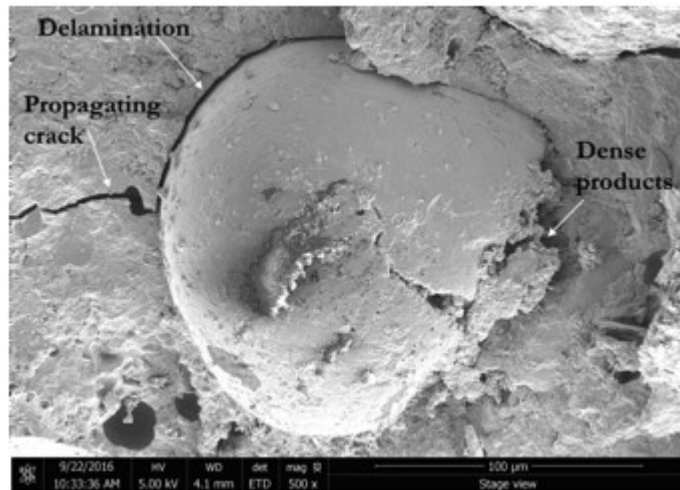
539 Extracted materials of the crack surface from both panels were observed using an SEM to
 540 characterise the healing products and typical images are presented in Fig. 19a-e. Fig. 19a shows
 541 multiple smooth cavities left by either debonded or ruptured microcapsules together with
 542 microcracks throughout the image attracted to, and passing through, the microcapsule locations.
 543 This is in agreement with previous observations whereby the presence of microcapsules were seen
 544 to provide a preferential path for cracks in mortar [21]. This phenomenon is considered beneficial
 545 for this self-healing system as it ensured microcapsules can be ruptured during crack propagation.
 546 Fig. 19b shows hexagonal calcium hydroxide crystals indicating their formation in the periphery of
 547 the microcapsules although on the crack surface, little, if any, can be seen. Instead, calcium
 548 carbonate and copious C-S-H flakes were observed. The former of these observations agree with
 549 previous findings that microcapsules act as nucleation sites for portlandite formation [43] whilst the
 550 latter of these products may be attributed to the reaction of the encapsulated sodium silicate with
 551 portlandite [39].

552 As the pieces of concrete material were extracted from near the crack mouth, the increased quantity
 553 of observed carbonation products is not surprising due to direct exposure to the external

554 environment and CO₂. SEM images also show products that have precipitated within small spherical
 555 voids of entrained air (Fig. 19b) suggesting that the products were generated following hardening of
 556 the concrete and most likely not produced during the initial cement hydration process. Ruptured
 557 microcapsules embedded on the crack surface could also be seen. In Fig. 19c, a crack approaching
 558 from the left-hand side is seen to pass through, or potentially debond, the microcapsule at this
 559 location. The stress concentration generated by the crack at this point was clearly not sufficient to
 560 rupture the microcapsule shell. However, on the right-hand side, the microcapsule shell is certainly
 561 ruptured and copious dense amorphous calcium silicate hydrate (C-S-H) phases are observed in the
 562 vicinity as suggested by the image brightness. In contrast, SEM images of samples extracted from the
 563 control panel (e.g. Fig. 19d and 19e) are consistently darker than those obtained from the
 564 microcapsule panel; indicating higher porosity in the matrix. The SEM images also show a variety of
 565 cement hydration products. Large calcium hydroxide crystals can be seen with other carbonation
 566 and C-S-H products on top. All of these SEM observations agree well with the expected autonomic
 567 self-healing mechanism whereby sodium silicate reacts with portlandite to produce C-S-H.

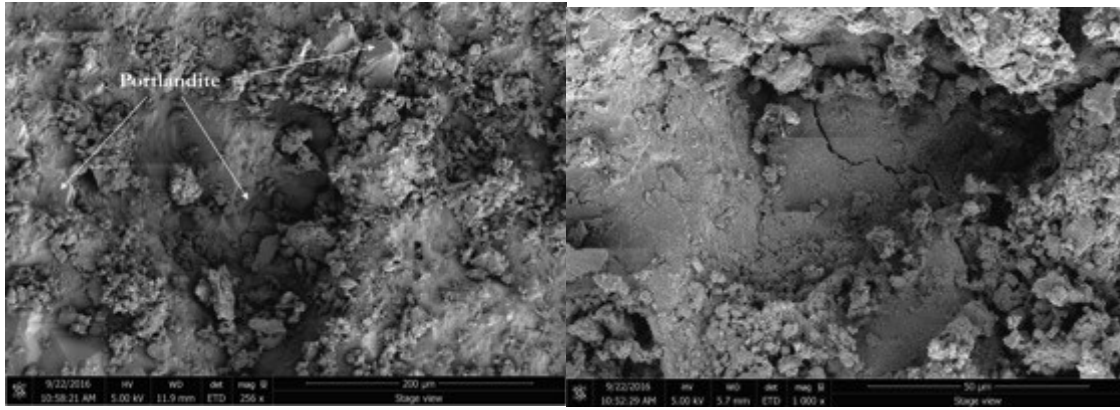


568 (a) (b)



570 (c)

571



(d)

(e)

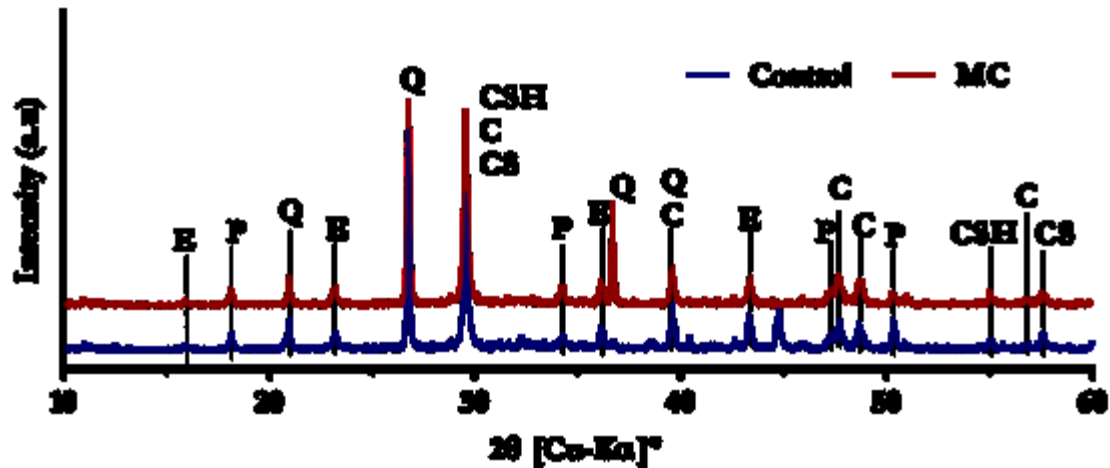
572

573

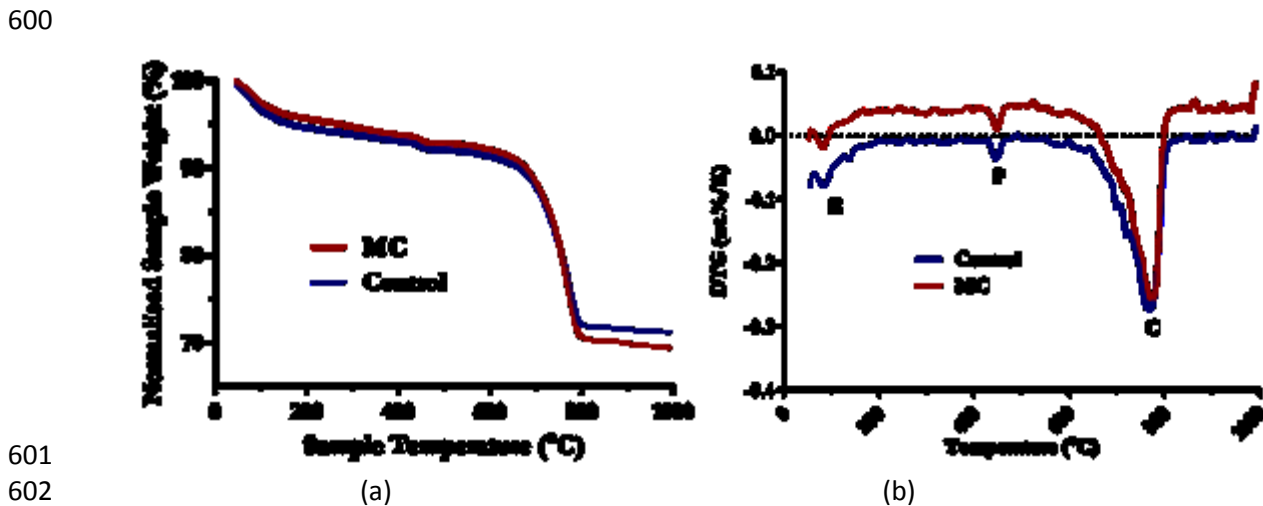
574 **Figure 19 Scanning electronic microscope (SEM) images from the MC and Control wall crack**
 575 **surfaces: (a) the attraction of microcracks towards microcapsule cavity locations; (b) crack surface**
 576 **adjacent to microcapsule cavity showing the deposition of carbonation and hydration products; (c)**
 577 **a ruptured microcapsule with dense hydration products at the outlet and (d, e) crack surface of**
 578 **the control wall showing high porosity and copious carbonation products.**

579

580 XRD spectra for material extracted from both the microcapsule and control wall cracks after
 581 reloading revealed the same crystalline materials within the powdered samples, e.g. portlandite C-H,
 582 calcite and broad C-S-H peaks, with marginal differences observed (Fig. 20). This confirms that
 583 similar products have formed in the cracks. TGA/DTG tests (Fig. 21) showed similar quantities of
 584 portlandite and calcite with the portlandite content being quite very small. This is consistent with
 585 the SEM observations and is expected as portlandite close to the wall surface will carbonate to
 586 produce calcite. As mentioned previously, it has been observed that the portlandite content in
 587 cementitious samples increases when microcapsules are added into the mixture. Therefore, before
 588 damage occurs, an increased quantity of portlandite in expected to exist within the MC wall
 589 compared with the Control wall. However, when damage occurs and microcapsules are ruptured,
 590 sodium silicate is released and reacts with portlandite to produce C-S-H. Therefore, the portlandite
 591 content within a crack, and particularly in the vicinity of microcapsules, should reduce. As a result,
 592 the similar quantities of portlandite measured could actually indirectly suggest that the autonomic
 593 self-healing reactions did take place. The larger quantities of calcite measured in samples extracted
 594 from the microcapsule wall also support these observations. The larger quantities suggest that a
 595 greater proportion of portlandite existed previously in this region and ultimately in the microcapsule
 596 wall.



597
 598 Figure 18 X-ray power diffraction (XRD) of powder extracted from MC and Control wall crack,
 599 where C: CaCO_3 , CS: $2\text{CaO}\cdot\text{SiO}_2$, $3\text{CaO}\cdot\text{SiO}_2$, CSH: $3\text{CaO}\cdot 2\text{SiO}_2\cdot 4\text{H}_2\text{O}$, P: $\text{Ca}(\text{OH})_2$ and Q: SiO_2 .



601
 602 (a) (b)
 603 Figure 19 Representative TGA/DTG graphs of powder extracted from crack faces of MC and control
 604 walls (a) TGA weight loss, (b) DTG curves where E: ettringite, P: portlandite and C: calcite

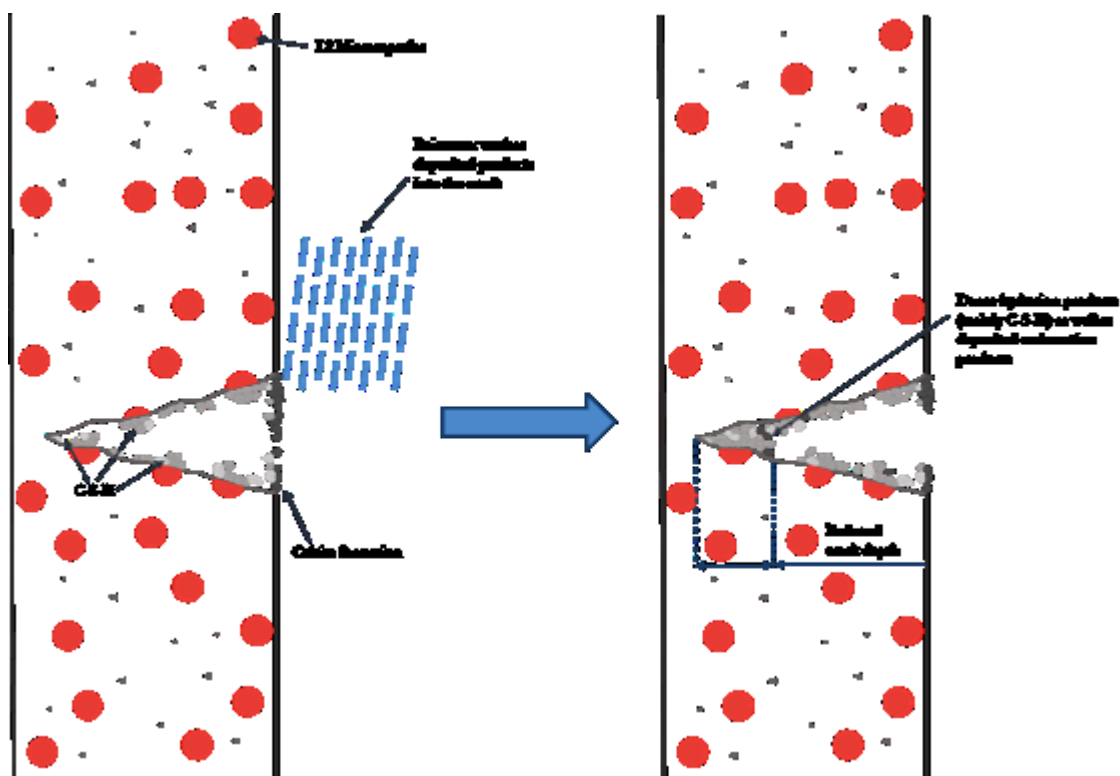
605 It is worth noting that it is difficult to distinguish between a reduction in portlandite due to reaction
 606 with the sodium silicate or carbonation to form calcite. However, these cumulative measurements
 607 support the hypothesis that a greater portlandite content existed in the microcapsule wall prior to
 608 cracking and has either been converted to calcite or reacted with the healing agent to form C-S-H.
 609 Furthermore, the increased quantity of calcite measured in the microcapsule wall sample is
 610 consistent with the increased visual healing that was observed at the crack mouth.

611
 612 **3.5 Healing mechanism**

613 Coupling non-destructive testing results with macroscopic and microscopic observations it is
 614 possible to theorise the self-healing mechanism that had taken place in both walls. In both walls, the
 615 observed width at the crack mouth consistently reduced between monitoring events #1 and #4,
 616 mainly due to the precipitation of calcite. These monitoring events took place between November
 617 and February whereby air temperatures gradually decreased and daily rainfall increased. However,
 618 between monitoring events #4 and #5, less carbonates filled the crack mouth and the measured
 619 crack width increased. It is believed that the increased rainfall washed products that had
 620 precipitated at the crack mouth deeper into the crack and towards the crack tip (shown
 621 schematically in Fig. 22). The crack depth measurements taken at monitoring event #5 (Fig. 16)

622 support this. However, the reduction in crack depth was also caused by autogenic healing at the
 623 crack tip. At this location, healing was most likely to occur due to the close proximity of fracture
 624 surfaces. TGA of healing products on the crack surface and at the crack mouth revealed the large
 625 quantity of calcite present. In particular, a greater quantity of calcite was observed in the
 626 microcapsule wall crack. This is in agreement with the crack width observations in which the
 627 microcapsule wall saw greater areal healing. Since greater quantities of calcite precipitated at the
 628 crack mouth, a greater amount was washed into the crack. Therefore, greater healing at the crack
 629 mouth resulted in greater healing at the crack tip. However, these results also showed that healing
 630 at the crack mouth did not necessarily correspond to healing inside the crack.

631 The significant reduction in crack depth in the microcapsule wall hence cannot be due to the
 632 deposition of calcite alone. As well as the contribution from autogenic healing, autonomic healing
 633 due to the release of microencapsulated sodium silicate occurred. Microcapsules on the crack
 634 surface that were embedded within the cementitious matrix showed rupture and formed dense
 635 hydration products at the outlet. TGA results also showed a greater degree of hydration for the
 636 microcapsule wall; suggesting more hydration processes had occurred in comparison with the
 637 Control panel. Finally, air permeability measurements taken around the crack location also showed
 638 significant healing for the microcapsule wall in comparison to almost no healing in the Control wall
 639 (Fig. 17). These results are particularly useful as they provide insight into the densification of the
 640 bulk material due to self-healing processes taking place internally at other microcrack locations.



641
 642 **Figure 22 Healing mechanism of concrete wall panels: Carbonation products at the crack mouth**
 643 **are washed into the crack. This, along with autogenic and autonomic healing along the crack**
 644 **length and tip lead to a reduction in crack depth measurements.**

645 4 Conclusions

646 The work presented here is part of the first major self-healing concrete site trial in the UK. It is the
 647 first successful attempt to scale up and implement self-healing concrete incorporating microcapsules
 648 on site. Self-healing concrete using microencapsulated sodium silicate was cast on-site in a retaining
 649 wall panel together with a control panel for comparison purposes. The walls were mechanically

650 cracked after 35 days of curing and then reloaded and monitored for self-healing over a 6-month
651 period using air permeability, crack depth and microscopic crack width measurements. Although the
652 addition of 8% microcapsules, by volume of the cement, was found to slightly reduce the mechanical
653 strength, the microcapsule wall showed improved crack-width reduction, crack-depth reduction and
654 recovery in permeability, confirming the real-time feasibility of microcapsule-based healing. In
655 particular:

- 656 • Accelerated crack healing along the main crack of 49% and 63% was evident as early as 14
657 days and 28 days for the microcapsule wall compared to 14% and 36% respectively for the
658 control.
- 659 • The average crack depth was also seen to reduce by ~8% and ~39% after 14 days in the
660 control and microcapsule walls respectively reaching a final ~20% and ~58% at the end of
661 the monitoring period.
- 662 • These results were further confirmed by significant permeability recovery (almost greater
663 than 2.5 orders of magnitude) for the microcapsule wall.
- 664 • A strength recovery of 25% was achieved in the microcapsule wall, achieving a 10%
665 improvement over the control panel.
- 666 • A temporal variation of the healing progression was identified in both panels influencing
667 final observations. Macroscopic observations showed some crack opening for both walls
668 following the initial reduction in crack width. Yet healing at the end of the monitoring period
669 for the microcapsule panel remained significantly higher compared to the control panel.
- 670 • Microscopic imaging and microstructural investigations of extracted samples from the crack
671 planes suggested a self-healing mechanism similar to what was observed in laboratory
672 investigations.
- 673 • μ CT confirmed the survivability and good distribution of microcapsules on site. SEM images
674 revealed dense products formed around embedded ruptured microcapsules confirming the
675 hypothesised release mechanism.
- 676 • TGA and XRD results of extracted material from the crack surfaces showed copious
677 carbonation products in both cases and increased quantities of calcium silicate hydrate (C-S-
678 H) in the microcapsule wall further supporting previous findings on the beneficial
679 contribution of the microencapsulated sodium silicate to the autonomic self-healing
680 progress.

681 Although the cast panels were not used in a structural application, this is a valuable step in gaining
682 the confidence of civil engineering contractors, designers and consultants to adopt disruptive
683 technologies working towards reducing and removing the requirement for inspection, maintenance
684 and repair of concrete structures.

685 Conflict of Interest

686 None.

687 Acknowledgements

688 The authors would like to thank all of those involved with the EPSRC Materials for Life (M4L) project;
689 in particular, Dr Robert Davies, Dr Martins Pilegis and Dr Oliver Teal for their contribution to the field
690 trials. The financial support from the EPSRC for the Materials for Life (M4L) project (EP/K026631/1)
691 and Resilient Materials for Life (RM4L) Programme Grant (EP/P02081X/1) is gratefully
692 acknowledged. The financial support from the EPSRC in the form of PhD studentships to Petros
693 Giannaros and Chrysoula Litina is also gratefully acknowledged.

694 References

695 [1] UK Treasury, National Infrastructure Delivery Plan 2016–2021, HM Treasury,

696 London, 2016. www.gov.uk/government/publications.

697 [2] ONS, Construction output in Great Britain: May 2016, (2016).
698 <https://www.ons.gov.uk/>.

699 [3] G. Tilly, J. Jacobs, Concrete repairs: Performance in service and current practice, BRE
700 Press, UK., 2007.

701 [4] World Economic Forum, The Boston Consulting Group, A Breakthrough in Mindset
702 and Technology - Shaping the Future of Construction, 2016.

703 [5] European Commission, Business Innovation Observatory - Smart Living: Advanced
704 Building Materials, 2014.

705 [6] Government Office For Science, Technology and Innovation Futures, 2017.

706 [7] i3P, Technology Roadmap for UK Construction & National Infrastructure, 2017.
707 [https://www.i3p.org.uk/wp-content/uploads/2017/07/i3P-CI-Technology-Roadmap-Booklet-](https://www.i3p.org.uk/wp-content/uploads/2017/07/i3P-CI-Technology-Roadmap-Booklet-FINAL.pdf)
708 [FINAL.pdf](https://www.i3p.org.uk/wp-content/uploads/2017/07/i3P-CI-Technology-Roadmap-Booklet-FINAL.pdf).

709 [8] M. de Rooij, K. Van Tittelboom, N. De Belie, E. Schlangen, Self-Healing Phenomena in
710 Cement-Based Materials State-of-the-Art Report of RILEM Technical Committee 221-SHC:
711 Self-Healing Phenomena in Cement-Based Materials, RILEM 2013, 2013.

712 [9] N. De Belie, E. Gruyaert, A. Al-Tabbaa, P. Antonaci, C. Baera, D. Bajare, A.
713 Darquennes, R. Davies, L. Ferrara, T. Jefferson, C. Litina, B. Miljevic, A. Otlewska, J. Ranogajec,
714 M. Roig-Flores, K. Paine, P. Lukowski, P. Serna, J.-M. Tulliani, S. Vucetic, J. Wang, H.M.
715 Jonkers, A Review of Self-Healing Concrete for Damage Management of Structures, *Adv.*
716 *Mater. Interfaces.* (2018) 1800074. doi:10.1002/admi.201800074.

717 [10] L.L. Souza, A. Al-Tabbaa, Microfluidic fabrication of microcapsules tailored for self-
718 healing in cementitious materials, *Constr. Build. Mater.* 184 (2018) 713–722.
719 doi:10.1016/J.CONBUILDMAT.2018.07.005.

720 [11] B. Boh, Boštjan Šumiga, B. Šumiga, Microencapsulation technology and its
721 applications in building construction materials, *RMZ - Mater. Geoenvironment.* 55 (2008)
722 329–344.

723 [12] S.R. White, N.R. Sottos, P.H. Geubelle, J.S. Moore, M.R. Kessler, S.R. Sriram, E.N.
724 Brown, S. Viswanathan, Autonomic healing of polymer composites., *Nature.* 409 (2001) 794–
725 7. doi:10.1038/35057232.

726 [13] M. Pelletier, R. Brown, A. Shukla, A. Bose, Self-healing concrete with a
727 microencapsulated healing agent, Kingston, USA, 2011.
728 [http://energetics.chm.uri.edu/system/files/Self healing concrete -7-11.pdf](http://energetics.chm.uri.edu/system/files/Self%20healing%20concrete%20-%207-11.pdf).%0A[9].

729 [14] Z. Yang, J. Hollar, X. He, X. Shi, A self-healing cementitious composite using oil
730 core/silica gel shell microcapsules, *Cem. Concr. Compos.* 33 (2011) 506–512.
731 doi:10.1016/j.cemconcomp.2011.01.010.

732 [15] L. Ferrara, T. Van Mullem, M.C. Alonso, P. Antonaci, R.P. Borg, E. Cuenca, A.
733 Jefferson, P.-L. Ng, A. Peled, M. Roig-Flores, M. Sanchez, C. Schroefl, P. Serna, D. Snoeck, J.M.
734 Tulliani, N. De Belie, Experimental characterization of the self-healing capacity of cement
735 based materials and its effects on the material performance: A state of the art report by COST
736 Action SARCOS WG2, *Constr. Build. Mater.* 167 (2018) 115–142.
737 doi:10.1016/j.conbuildmat.2018.01.143.

738 [16] A. Kanellopoulos, T.S. Qureshi, A. Al-Tabbaa, Glass encapsulated minerals for self-
739 healing in cement based composites, *Constr. Build. Mater.* 98 (2015) 780–791.
740 doi:10.1016/j.conbuildmat.2015.08.127.

741 [17] T.S. Qureshi, A. Kanellopoulos, A. Al-Tabbaa, Encapsulation of expansive powder
742 minerals within a concentric glass capsule system for self-healing concrete, *Constr. Build.*
743 *Mater.* 121 (2016) 629–643. doi:10.1016/J.CONBUILDMAT.2016.06.030.

744 [18] C. Litina, A. Kanellopoulos, A. Al-Tabbaa, Alternative repair system for concrete using
745 microencapsulated healing agents, in: M. Grantham, M. Basheer, B. Magee, M. Soutsos
746 (Eds.), *Proc. Concr. Solut. 5th Int. Conf. Concr. Repair*, Taylor & Francis Group, Belfast, 2014:

747 pp. 97–103.

748 [19] A. Kanellopoulos, P. Giannaros, D. Palmer, A. Kerr, A. Al-Tabbaa, Polymeric
749 microcapsules with switchable mechanical properties for self-healing concrete: synthesis,
750 characterisation and proof of concept, *Smart Mater. Struct.* 26 (2017) 045025.
751 doi:10.1088/1361-665X/aa516c.

752 [20] P. Giannaros, A. Kanellopoulos, A. Al-Tabbaa, Sealing of cracks in cement using
753 microencapsulated sodium silicate, *Smart Mater. Struct.* 25 (2016) 084005.
754 doi:10.1088/0964-1726/25/8/084005.

755 [21] A. Kanellopoulos, P. Giannaros, A. Al-Tabbaa, The effect of varying volume fraction
756 of microcapsules on fresh, mechanical and self-healing properties of mortars, *Constr. Build.
757 Mater.* 122 (2016) 577–593. doi:10.1016/j.conbuildmat.2016.06.119.

758 [22] C.M. Dry, Repair and prevention of damage due to transverse shrinkage cracks in
759 bridge decks, 1999 Symp. *Smart Struct. Mater.* 3671 (1999) 253–256.

760 [23] T.D.P. Thao, Quasi-brittle self-healing materials: numerical modelling and
761 applications in civil engineering, PhD Thesis National University of Singapore, 2011.

762 [24] G. Karaiskos, E. Tsangouri, D.G. Aggelis, K. Van Tittelboom, N. De Belie, D. Van
763 Hemelrijck, Performance monitoring of large-scale autonomously healed concrete beams
764 under four-point bending through multiple non-destructive testing methods, *Smart Mater.
765 Struct.* 25 (2016). doi:10.1088/0964-1726/25/5/055003.

766 [25] C. Dry, IN-SERVICE REPAIR OF HIGHWAY BRIDGES AND PAVEMENTS BY INTERNAL
767 TIME-RELEASE REPAIR CHEMICALS, NCHRP-IDEA Progr. Proj. Final Rep. (2001).
768 <https://trid.trb.org/view.aspx?id=692570> (accessed October 24, 2017).

769 [26] C.M. Dry, Self-repair of cracks in brittle material systems, in: SPIE 9800, *Behav.
770 Mech. Multifunct. Mater. Compos.* 2016, Las Vegas, 2016. doi:10.1117/12.2218564.

771 [27] H.M. Jonkers, E. Schlangen, Self-healing of cracked concrete: A bacterial approach,
772 6th Int. Conf. *Fract. Mech. Concr. Struct.* 3 (2007) 1821–1826.

773 [28] E. Tziviloglou, V. Wiktor, H.M. Jonkers, E. Schlangen, Bacteria-based self-healing
774 concrete to increase liquid tightness of cracks, *Constr. Build. Mater.* 122 (2016) 118–125.
775 doi:10.1016/j.conbuildmat.2016.06.080.

776 [29] M.G. Sierra-Beltran, H.M. Jonkers, M. Ortiz, Field application of self-healing
777 concrete with natural fibres as linings for irrigation canals in Ecuador, *Fifth Int. Conf. Self-
778 Healing Mater.* (2015) 32.

779 [30] A. Stewart, The ‘living concrete’ that can heal itself, CNN. (2016).
780 <https://edition.cnn.com/2015/05/14/tech/bioconcrete-delft-jonkers/index.html>.

781 [31] K. Paine, R. Lark, A. Al-Tabbaa, Biomimetic multi-scale damage immunity for
782 concrete, in: UKIERI *Concr. Congr. Concr. Res. Driv. Profit Sustain.*, Jalandhar (Punjab), India,
783 2015. <http://opus.bath.ac.uk/48322/>.

784 [32] R.J. Lark, A. Al-Tabbaa, K. Paine, Biomimetic multi-scale damage immunity for
785 construction materials : M4L Project overview, in: 4th Int. Conf. *Self-Healing Mater.*, Ghent,
786 2013: pp. 2–5.

787 [33] A. Al-Tabbaa, B. Lark, K. Paine, T. Jefferson, C. Litina, D. Gardner, T. Embley,
788 Biomimetic Cementitious Construction Materials for Next Generation Infrastructure, *Proc.
789 Inst. Civ. Eng. - Smart Infrastruct. Constr.* (2018) 1–35. doi:10.1680/jsmic.18.00005.

790 [34] O. Teall, R. Davies, M. Pilegis, A. Kanellopoulos, T. Sharma, K. Paine, A. Jefferson, R.
791 Lark, D. Gardner, A. Al-Tabbaa, Self-healing concrete full-scale site trials, in: K. Maekawa, A.
792 Kasuga, J. Yamazaki (Eds.), *Proc. 11th Fib Int. PhD Symp. Civ. Eng.*, Tokyo, Japan, 2016: pp.
793 639–646.

794 [35] R. Davies, O. Teall, M. Pilegis, A. Kanellopoulos, T. Sharma, A. Jefferson, D. Gardner,
795 A. Al-Tabbaa, K. Paine, R.J. Lark, Large Scale Application of Self-Healing Concrete: Design,
796 Construction and Testing, *Front. Mater.* 5 (2018) 51. doi:10.3389/FMATS.2018.00051.

797 [36] P. Giannaros, A. Kanellopoulos, A. Al-Tabbaa, Damage recovery in self-healing

798 concrete, in: Heal. Conf., Delft, The Netherlands, 2016.
799 [37] R.J. Torrent, A two-chamber vacuum cell for measuring the coefficient of
800 permeability to air of the concrete cover on site, *Mater. Struct.* 25 (1992) 358–365.
801 doi:10.1007/BF02472595.
802 [38] R. Alghamri, A. Kanellopoulos, A. Al-Tabbaa, Impregnation and encapsulation of
803 lightweight aggregates for self-healing concrete, *Constr. Build. Mater.* 124 (2016) 910–921.
804 doi:10.1016/j.conbuildmat.2016.07.143.
805 [39] S. Irico, A. Bovio, G. Paul, E. Boccaleri, D. Gastaldi, L. Marchese, L. Buzzi, F. Canonico,
806 A solid-state NMR and X-ray powder diffraction investigation of the binding mechanism for
807 self-healing cementitious materials design: The assessment of the reactivity of sodium silicate
808 based systems, *Cem. Concr. Compos.* (2016). doi:10.1016/j.cemconcomp.2016.11.006.
809 [40] S. Jacobsen, J. Marchand, H. Hornain, Sem observations of the microstructure of
810 frost deteriorated and self-healed concretes, *Cem. Concr. Res.* 25 (1995) 1781–1790.
811 doi:10.1016/0008-8846(95)00174-3.
812 [41] C. Edvardsen, Water permeability and autogenous healing of cracks in concrete, *ACI*
813 *Mater. J.* 96-M56 (1999) 448–454.
814 [42] L. Ebensperger, R. Torrent, Concrete air permeability “in situ” test: status quo, *Rev.*
815 *Ing. Construcción.* 25 (2011) 371–382.
816 [43] M. Aguayo, S. Das, A. Maroli, N. Kabay, J.C.E. Mertens, S.D. Rajan, G. Sant, N.
817 Chawla, N. Neithalath, The influence of microencapsulated phase change material (PCM)
818 characteristics on the microstructure and strength of cementitious composites: Experiments
819 and finite element simulations, *Cem. Concr. Compos.* 73 (2016) 29–41.
820 doi:10.1016/j.cemconcomp.2016.06.018.
821